EFFECTS OF SOLID STATE POWER AMPLIFIER NONLINEARITY ON VARIOUS PHASE SHIFT KEYING MODULATION SCHEMES

A THESIS SUBMITTED TO
THE GRADUATE SCHOOL OF NATURAL AND APPLIED SCIENCES
OF
MIDDLE EAST TECHNICAL UNIVERSITY

BY

CELAL DUDAK

IN PARTIAL FULFILLMENT OF THE REQUIREMENTS
FOR
THE DEGREE OF MASTER OF SCIENCE
IN
ELECTRICAL AND ELECTRONICS ENGINEERING

JANUARY 2005

Approval of the Graduate School of Natural and Applied Sciences

_____

Prof. Dr. Canan ÖZGEN

Director

I certify that this thesis satisfies all the requirements as a thesis for the degree of Master of Science.

_____

Prof. Dr. İsmet ERKMEN

Head of Department

This is to certify that we have read this thesis and that in our opinion it is fully adequate, in scope and quality, as a thesis for the degree of Master of Science.

_____	_____
Assoc. Prof. Dr. Sencer KOÇ	Assist. Prof Dr. Arzu TUNCAY KOÇ
Co-Supervisor	Supervisor

Examinig Comitee Members

Prof. Dr. Yalçın TANIK	(METU, EE)	_____
Assist. Prof. Dr. Arzu TUNCAY KOÇ	(METU, EE)	_____
Assoc. Prof. Dr. Sencer KOÇ	(METU, EE)	_____
Assist. Prof. Dr. Ali Özgür YILMAZ	(METU, EE)	_____
Dr. Özlem APAYDIN ŞEN	(TÜBİTAK)	_____

I hereby declare that all information in this document has been obtained and presented in accordance wtih academic rules and ethical conduct. I also declare that, as required by these rules and conduct, I have fully cited and referenced all material and results that are not original to this work.

Celal DUDAK

ABSTRACT

EFFECTS OF SOLID STATE POWER AMPLIFIER NONLINEARITY ON VARIOUS PHASE SHIFT KEYING MODULATION SCHEMES

Dudak, Celal

M.Sc., Department of Electrical and Electronics Engineering

Supervisor: Assist. Prof. Dr. Arzu Tuncay Koç

Co-supervisor: Assoc. Prof. Dr. Sencer Koç

January 2005, 90 pages

This study concentrates on the performance evaluation of a specific modulation scheme under nonlinear operation. This modulation scheme is the phase shift keying (PSK) modulation, exemplified by the special cases of BPSK, QPSK, OQPSK, $\pi/4$-QPSK. The specific nonlinear block is chosen to be the solid state power amplifier (SSPA) structure whose simulation model is the Rapp model. Varying transmitter filter characteristic and one of the power amplifier parameters constitute the main methodology of simulations. Bit error rate (BER), error vector magnitude (EVM), and Space Frequency Coordination Group (SFCG) spectral mask constraint are the

evaluation parameters taken into account throughout this study. Simulation results support the initial literature survey, which reveals additional features showing how each modulation scheme is affected by various SSPA nonlinearity characteristics.

Keywords: PSK, SSPA, Rapp, Nonlinearity, BER, EVM

ÖZ

KATI HAL GÜÇ YÜKSELTECİ DOĞRUSALSIZLIĞININ ÇEŞİTLİ EVRE KAYDIRMALI KİPLENİM TASLAKLARI ÜZERİNE ETKİLERİ

Dudak, Celal

Yüksek Lisans, Elektrik ve Elektronik Mühendisliği Bölümü

Tez Yöneticisi: Yard. Prof. Dr. Arzu T. Koç

Yardımcı Tez Yöneticesi: Assoc. Prof. Dr. Sencer Koç

Ocak 2005, 90 sayfa

Bu tez, özgül bir kiplenim taslağının doğrusal olmayan çalışma koşulları altındaki performans değerlendirmesini sunar. Bu kiplenim biçimi, BPSK, QPSK, OQPSK ve π/4-QPSK özel durumlarıyla örneklenen evre kaydırmalı kiplenim (PSK) olarak belirlenmiştir. Bu halde özgül doğrusal olmayan blok, benzetim modeli Rapp model olan katı hal güç yükselteci olarak seçilmiştir. Verici süzgeç özelliğinin ve güç yükselteci parametrelerinden birinin değiştirilmesi, benzetimlerdeki ana yöntemi oluşturmaktadır. Bit hata oranı (BER), hata vektörü büyüklüğü (EVM) ve Uzay Frekans Koordinasyon Grubu (SFCG) spektral maske kısıtı, ele alınan

değerlendirme parametrelerini oluşturmaktadır. Benzetim sonuçları başlangıçtaki literatür araştırmasını, her kiplenim taslağının çeşitli doğrusal olmayan SSPA özgüllükleri tarafından nasıl etkilendiğini göstererek, desteklemektedir.

Anahtar Sözcükler: PSK, SSPA, Rapp, Doğrusalsızlık, BER, EVM

ACKNOWLEDGMENTS

I am very grateful to my supervisor Assist. Prof. Dr. Arzu Tuncay Koç for her endless support and encouragement throughout this study. She has always been patient and motivative at all the stages of this thesis.

I would like to express my appreciation to my co-supervisor Assoc. Prof. Dr. Sencer Koç for his guidance and helpful comments in the development of this thesis.

I would also like to thank to Özlem Şen in TÜBİTAK-ODTÜ-BİLTEN for the inspiration and help she gave. I also wish to thank to my workplace coordinator Hacer K. Sunay for her interests throughout my thesis.

And finally, I would like to express very special gratitudes to my dear mother, father and sister, for their patience, love and encouragement that they demonstrated during my studies.

To my dear family.

TABLE OF CONTENTS

LIST OF TABLES

TABLE

LIST OF FIGURES

FIGURE

CHAPTER 1

INTRODUCTION

In the last century, telecommunication has gained an indispensable place nearly in all areas of the public life. Especially, the field of digital communications, which constitutes a huge leap against analog communication, is in a tremendous ascent since the publication of C.E. Shannon's work over 50 years ago [1].

Scientists and engineers studying in this area are still trying to improve the quality of telecommunication [2], which becomes mutilated with the existence of natural communication media problems, i.e., noise and fading. Besides, problems arising from human intentions are also self-evident, i.e., types of interferences. Nonlinearity is judged to be in between two, which is known as a type of input-output power relation form in electrical devices [3]. It is known to be a controllable phenomenon depending on the power level of the input signal in these devices [4].

Nonlinearity is also observed in the process of communication signal forming. Namely, every signal forming structure found in the practical communication transmitters can operate more or less in a nonlinear fashion. Though, the principal device which should be thought in this context is the power amplifier which takes part at the end of the communication transmitter line-up.

There are various power amplifier types utilized in the transmitters to boost up the power level of the communication signal where main ones are travelling wave tube amplifiers (TWTA) [5] and solid state power amplifiers (SSPA) [6]. These devices

are commonly operated at the edge to acquire a high power level at the output to satisy the communication link constraints and high efficiency requirements. Meanwhile, the carefully modulated and filtered communication signal faces an irreversible nonlinear distortion arising from this strain. In literature [7-9], these distortion researches more frequently concentrate on the adjacent channel power [7] phenomenon due to the urgent needs of terrestial applications, e.g., GSM. This need stems from the fact that utilized terrestial links are frequently band-limited [10], that is they should support reliable multi-user communication. Space communication links are rather power limited [10], where they additionally require high data rates with high communication quality, which can be quantified with various error rates.

Small number of analysis of nonlinear distortions on the signal modulation quality in the space applications constituted the main motivation for the study. Hence, throughout this thesis, the consequences of this distortion is attempted to be investigated thoroughly, in the specific case of utilizing SSPA as power boosting nonlinear device. As the modulation format to be affected by the nonlinearity, several specific phase shift keying (PSK) modulation schemes, namely BPSK, QPSK, OQPSK, $\pi/4$-QPSK, are chosen, being the primary modulation formats preferred in space communications. Continuous Phase Modulation (CPM) schemes (e.g., MSK) are not considered as the modulation format throughout this study since the analysis is based on a present communication transmitter which utilizes PSK schemes.

Chapter 2, hence, summarizes these PSK modulation formats. Chapter 3 gives the theory of modeling process of nonlinear systems for simulation and exemplifies this topic with realizing the modeling of an SSPA designed at TÜBİTAK-ODTÜ-BİLTEN. Chapter 4 introduces, completely, the methodology utilized in the evaluation of performances of these PSK modulation formats under nonlinear operation. Finally, Chapter 5 gives the results and necessary discussions. Finally, concluding remarks are given in Chapter 6.

CHAPTER 2

THEORETHICAL BACKGROUND OF PHASE SHIFT KEYING TYPE MODULATION SCHEMES

2.1 Introduction

In the first years of deep space program, phase shift keying (PSK) is developed for it offers low probability of error and, yet, high bandwidth efficiency. It is now widely used in both military and commercial communications systems.

The general analytical expression for PSK can be given by [11]

$$s_i(t) = \sqrt{\frac{2E}{T}} \cos\left[2\pi f_c t + \phi_i(t)\right] \qquad \begin{array}{l} 0 \le t \le T, \\ i = 1,...,M \end{array} \qquad (2.1)$$

where E is the transmitted signal energy per symbol, T is the symbol duration, and f_c is the carrier frequency that is chosen equal to n_c/T for some fixed positive integer n_c. $\phi_i(t)$ denotes the phase of the modulated signal, which will have M discrete values according to

$$\phi_i(t) = \frac{2\pi}{M}(i-1) \qquad i = 1,2,...,M \qquad (2.2)$$

M is the number of allowable phase states of the signal and the resultant scheme is called M-ary PSK. During rest of this chapter, details for modulation and

demodulation of four selected PSK modulation schemes, namely, BPSK, QPSK, OQPSK and π/4-QPSK, are given.

2.2 Binary Phase Shift Keying

2.2.1 Signaling and Modulation

The resulting modulation technique is called binary phase shift keying (BPSK) when M=2. This means a symbol information corresponds to a bit information as T=T_b and E=E_b, in (2.1). Hence, there is a pair of signals, $s_1(t)$ and $s_2(t)$ as

$$s_1(t) = \sqrt{\frac{2E_b}{T_b}} \cos(2\pi f_c t) \qquad 0 \le t \le T_b \tag{2. 3}$$

$$s_2(t) = \sqrt{\frac{2E_b}{T_b}} \cos(2\pi f_c t + \pi) = -\sqrt{\frac{2E_b}{T_b}} \cos(2\pi f_c t) \qquad 0 \le t \le T_b \tag{2. 4}$$

In BPSK modulation, modulating data signal shifts the phase of the waveform $s_i(t)$ to one of two states, either zero or π radians (180°). Here, it is clear that there is only one basis function of unit energy, namely

$$\Theta_1(t) = \sqrt{\frac{2}{T_b}} \cos(2\pi f_c t) \qquad 0 \le t \le T_b \tag{2. 5}$$

Consequently, we may express the transmitted signals $s_1(t)$ and $s_2(t)$ in terms of $\Theta_1(t)$ as

$$s_1(t) = \sqrt{E_b} \cdot \Theta_1(t) \tag{2. 6}$$

$$s_2(t) = -\sqrt{E_b} \cdot \Theta_1(t) \tag{2. 7}$$

In order to generate the BPSK signal, the binary data is converted to polar format with constant amplitude levels of $+\sqrt{E_b}$ and $-\sqrt{E_b}$. This binary wave and sinusoidal wave, $\Theta_1(t)$, are applied to a product block as in Figure 2.1.

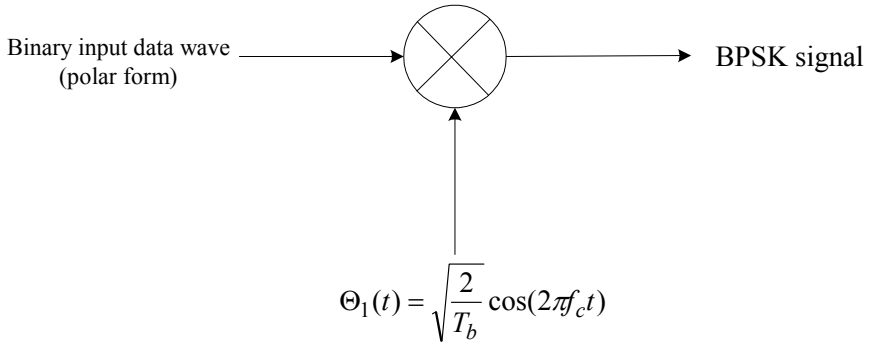

Figure 2.1 BPSK Modulator [12]

2.2.2 Coherent Demodulation

The correlation of resulting signal, $x(t)$ — that has experienced the channel — with the basis function $\Theta_1(t)$ has to be determined for demodulation process as in Figure 2.2. The output of the correlation is the observation element x_1, given as

$$x_1 = \int_0^{T_b} x(t)\Theta_1(t)dt \qquad (2.\ 8)$$

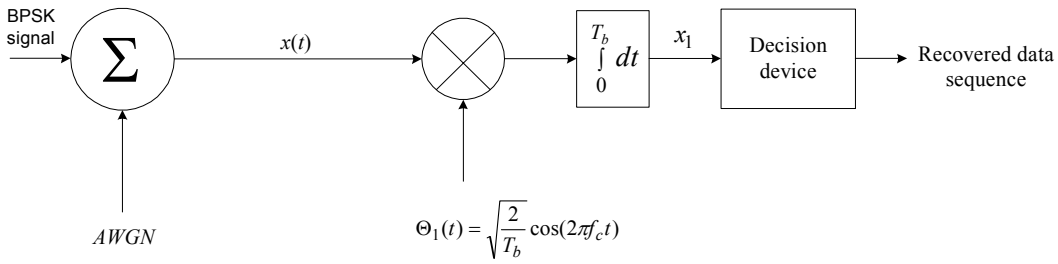

Figure 2.2 Coherent BPSK demodulator [12]

The bit error ratio for coherent BPSK demodulation can be calculated as [12]

$$P_b = \frac{1}{2}\text{erfc}\left(\sqrt{\frac{E_b}{N_o}}\right) \tag{2. 9}$$

where N_0 denotes power spectral density of AWGN and complementary error function (erfc) is given as

$$\text{erfc}(u) = \frac{2}{\sqrt{\pi}}\int_u^{\infty}\exp(-z^2)dz \tag{2. 10}$$

2.3 Quadriphase Shift Keying

One of the important properties of modulation schemes is their optimization capability of the efficient use of the channel bandwidth while minimizing transmitted power. This provides the motivation for the search for spectrally efficient modulation schemes which maximize the bandwidth efficiency. The latter quantity is the ratio of data rate to channel bandwidth for a specified probability of symbol error, [12].

In this section, quadriphase shift keying (QPSK) is introduced, being one of spectrally efficient PSK modulation schemes.

2.3.1 Signaling and Modulation

In QPSK modulation, the phase of the carrier takes on four possible values as

$$\phi_i(t) = (2i-1)\frac{\pi}{4} \qquad i = 1,2,3,4 \tag{2.11}$$

If this is inserted in (2.1) and a well-known trigonometric identity is used, the signal, $s_i(t)$, can be expressed as

$$s_i(t) = \sqrt{\frac{2E}{T}}\cos\left[(2i-1)\frac{\pi}{4}\right]\cos(2\pi f_c t) - \sqrt{\frac{2E}{T}}\sin\left[(2i-1)\frac{\pi}{4}\right]\sin(2\pi f_c t) \quad \begin{matrix} 0 \le t \le T \\ i = 1,\ldots,4 \end{matrix} \tag{2.12}$$

where $E=2E_b$ and $T=2T_b$, where each symbol (phase value) corresponds to a unique pair of bits (dibit). In the above equation, there are two quadrature carriers, hence there are two orthonormal basis functions, $\Theta_1(t)$ and $\Theta_2(t)$, which are shown below [12]

$$\Theta_1(t) = \sqrt{\frac{2}{T}}\cos(2\pi f_c t) \qquad 0 \le t \le T \tag{2.13}$$

$$\Theta_2(t) = -\sqrt{\frac{2}{T}}\sin(2\pi f_c t) \qquad 0 \le t \le T \tag{2.14}$$

Having two basis functions, the signal space diagram of QPSK is two dimensional with four message points (see Figure 2.3). Phase transitions are also shown in this figure. Since equivalent bit error probability for QPSK depends on the mapping of dibits into the corresponding signal phases, the preferred assignment is one in which adjacent phases differ by one binary digit. It is important in the demodulation of the signal because the most likely errors caused by noise involve the erroneous selection of an adjacent phase to the transmitted signal phase. This mapping is called *Gray encoding*, [2]. Signal space characterization showing this mapping procedure is given in Table 2.1.

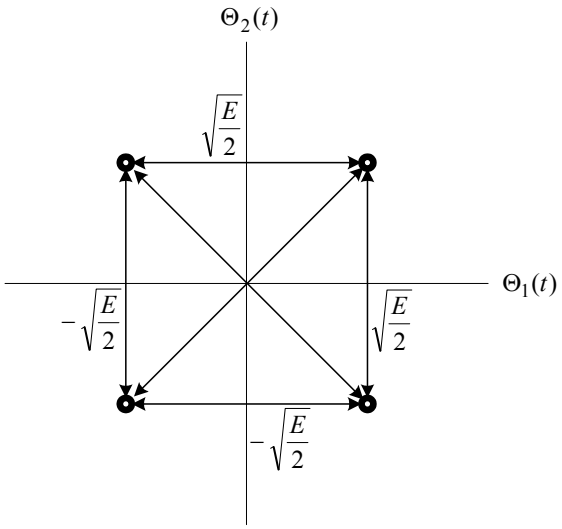

Figure 2.3 Signal space diagram of QPSK with signal constellation transitions [12]

Table 2.1 Signal space characterization of QPSK [12]

Information dibit	Phase of QPSK signal
10	$\pi / 4$
00	$3\pi / 4$
01	$5\pi / 4$
11	$7\pi / 4$

In order to generate the QPSK signal, the binary data are converted to polar format with constant amplitude levels of $+\sqrt{E_b}$ and $-\sqrt{E_b}$. Then, by means of a demultiplexer, data are divided into two separate data sequences consisting of the odd- and even-numbered input bits. These data streams are used to modulate a pair of orthonormal basis functions $\Theta_1(t)$ and $\Theta_2(t)$ (see Figure 2.4).

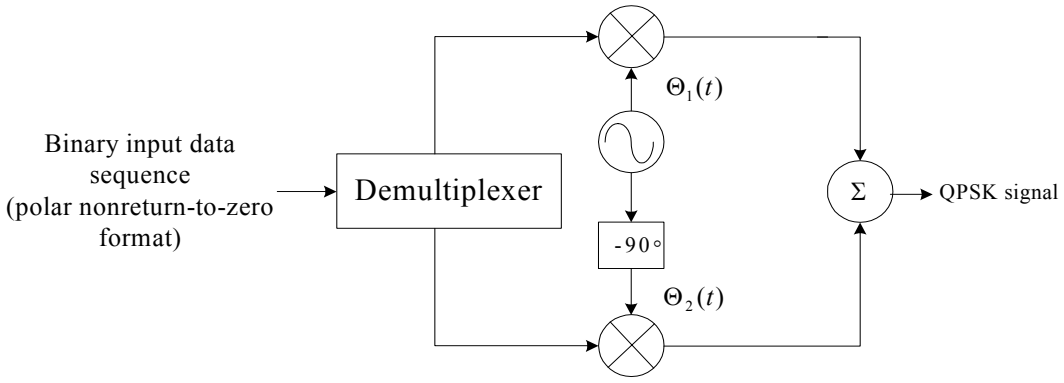

Figure 2.4 QPSK Modulator [12]

2.3.2 Coherent Demodulation

The coherent QPSK demodulator shown in Figure 2.5 consists of a pair of correlators driven by the basis functions $\Theta_1(t)$ and $\Theta_2(t)$. The correlator outputs x_1 and x_2 are the observation variables, which are followed by the decision devices. Therefore, the coherent QPSK demodulator can be considered as two coherent BPSK demodulators, using orthogonal carriers while working in parallel, [12].

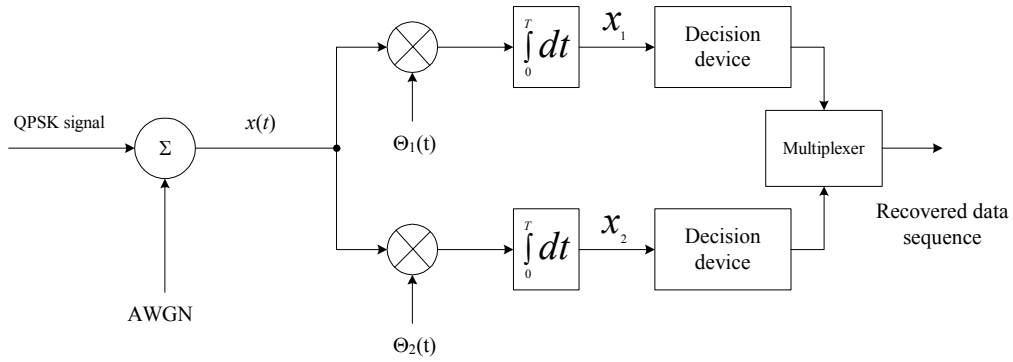

Figure 2.5 Coherent QPSK Demodulator [12]

With this structure and Gray encoding used for the incoming dibits (symbols), we find that the bit error ratio of QPSK is exactly

$$P_b = \frac{1}{2}\operatorname{erfc}\left(\sqrt{\frac{E_b}{N_0}}\right) \tag{2. 15}$$

A coherent QPSK system has the same average probability of bit error as a coherent BPSK system for the same bit rate and the same E_b/N_0, but uses only half the channel bandwidth, [12].

2.4 Offset QPSK

An alternative to conventional QPSK modulation scheme is offset QPSK (OQPSK), where quadrature arm is delayed by half symbol duration. This would result in that phase changes will occur twice as often in this new scheme. Oncoming subsections will describe this situation, introducing modulation and coherent demodulation of OQPSK.

2.4.1 Signaling and Modulation

In OQPSK modulation, the phase of the carrier takes on four possible values similar to QPSK. The modulated signal can be represented by [13]

$$s_i(t) = \sqrt{\frac{2E}{T}}\left\{m_I(t)\cos\left[2\pi f_c t + \phi_i(t)\right] + m_Q(t)\sin\left[2\pi f_c t + \phi_i(t)\right]\right\} \quad \begin{matrix} 0 \le t \le T \\ i = 1,...,4 \end{matrix} \tag{2. 16}$$

where $m_I(t)$ and $m_Q(t)$ denote the data carrying parts of the signal and are given by

$$m_I(t) = \sum_{k=-\infty}^{\infty} d_I\, p(t - kT) \tag{2. 17}$$

$$m_Q(t) = \sum_{k=-\infty}^{\infty} d_Q\, p(t - (k + \frac{1}{2})T) \tag{2. 18}$$

where d_I and d_Q denote the independent and identically distributed (i.i.d) binary (+1,-1) I and Q data streams. $p(t)$ is the pulse shape implemented prior to the demultiplexer, an example of which is used (root raised cosine filter) in the further study and is extensively described in Appendix A.

The signal space diagram of the OQPSK (see Figure 2.6) is the same as that of QPSK (given in Figure 2.3). The main difference is the elimination of possible state changes passing through the origin – meaning that signal amplitude goes to zero. That is, because of the inserted delay to quadrature arm, maximum phase transition is decreased to π/2 radians in OQPSK, whereas the same quantity is π radians in QPSK. Modulator topology of OQPSK is also given in Figure 2.7.

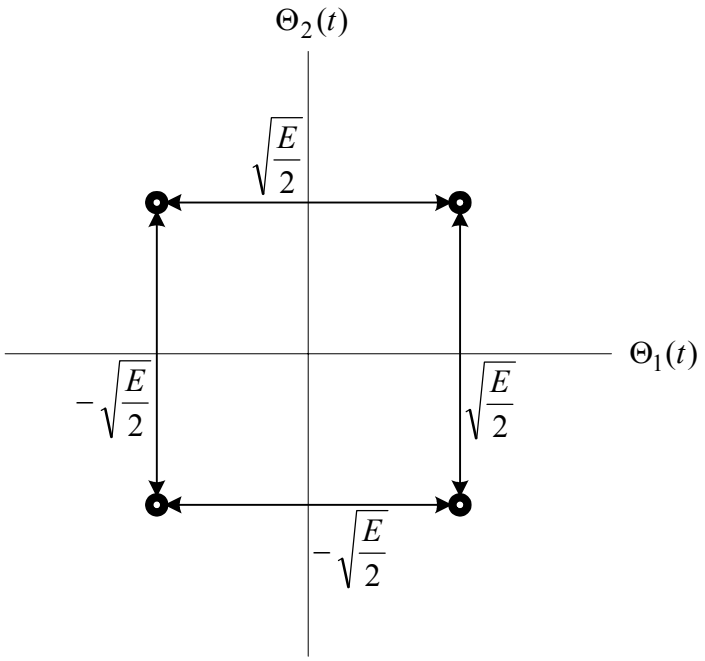

Figure 2.6 Signal space diagram of OQPSK with signal constellation transitions [13]

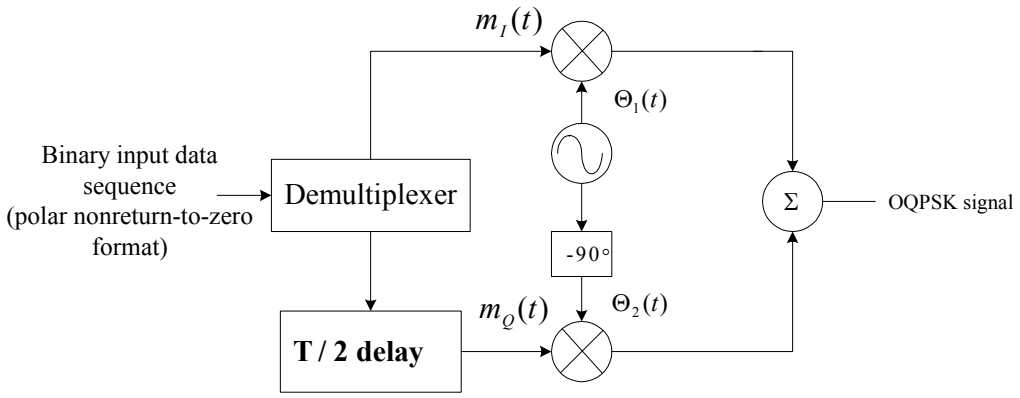

Figure 2.7 OQPSK modulator [14]

2.4.2 Coherent Demodulation

The coherent demodulator for OQPSK, which is illustrated in Figure 2.8, is very similar to the corresponding one of the QPSK. The extra half symbol delay inserted to the in-phase arm is used to compensate the delay at the modulator, [14]. The bit error ratio performance of OQPSK is exactly identical to that of QPSK, given in (2.15).

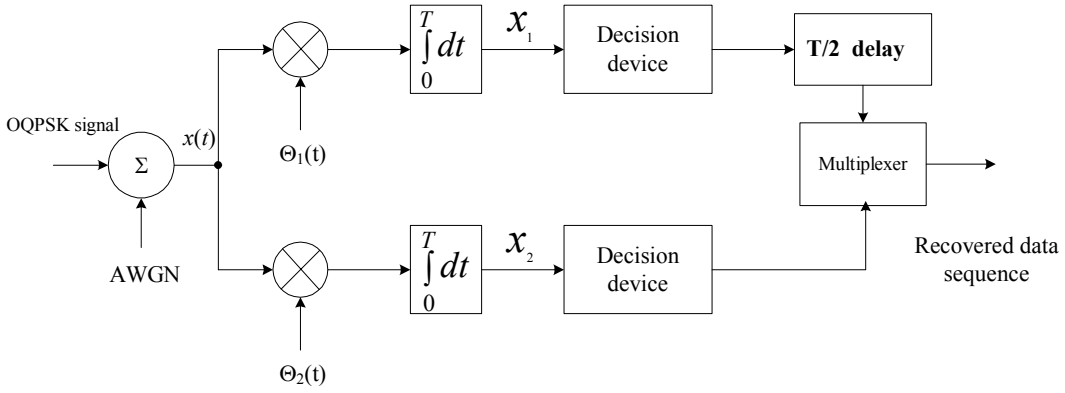

Figure 2.8 Coherent OQPSK demodulator [14]

2.5 Π/4-QPSK

Another variant of QPSK is π/4-QPSK. Maximum phase transition is decreased to 3π/4 radians compared to π radians of QPSK. Next subsections will introduce modulation and coherent differential demodulation of π/4-QPSK.

2.5.1 Signaling and Modulation

A block diagram of the transmitter is shown in Figure 2.9, where the transmitted signal is given by

$$s_k(t) = Au_k \cos(2\pi f_c t) - Av_k \sin(2\pi f_c t) \qquad kT \le t \le (k+1)T \qquad (2.\ 19)$$

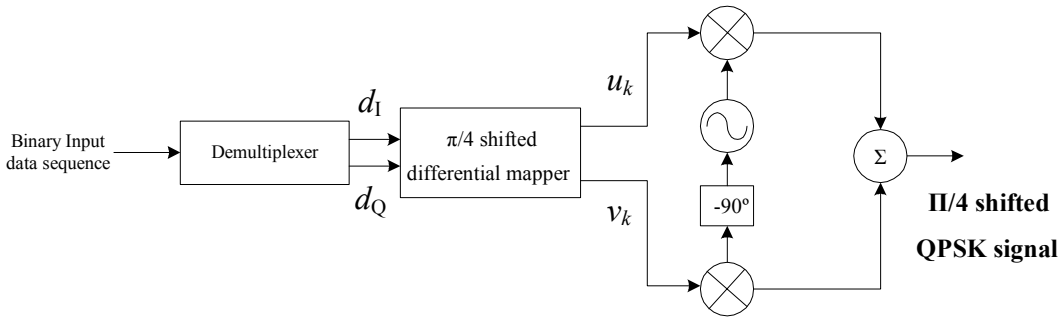

Figure 2.9 π/4 shifted QPSK modulator [14]

In this figure, d_I and d_Q are demultiplexed binary input data sequences. The output variables of the mapper block (u_k,v_k) are formulated by

$$u_k = u_{k-1}\cos\theta_k - v_{k-1}\sin\theta_k \qquad (2.\ 20)$$

$$v_k = u_{k-1}\sin\theta_k + v_{k-1}\cos\theta_k \qquad (2.\ 21)$$

and take values in the set of $\{0,\pm 1,\pm \sqrt{2}/2\}$. θ_k is related to the input bit pair (d_I,d_Q) as given in Table 2.2.

Table 2.2 Phase shift as a function of information dibit

Information dibit	θ
00	π/4
01	3π /4
11	-3π /4
10	-π /4

A deeper analytical study on this scheme shows that the transmitted signal is chosen alternatively from one of two QPSK constellations one rotated from the other by π/4 radians (see Figure 2.10). Hence, transitions from one constellation to another can have values in the set $\{\pm\pi/4, \pm 3\pi/4\}$.

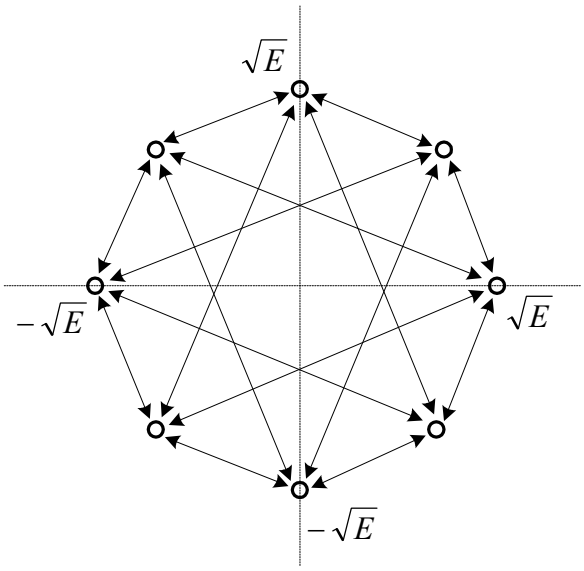

Figure 2.10 Signal space diagram and trajectories for π/4-QPSK [4]

2.5.2 Coherent Differential Demodulation

For the demodulation process, it turns out that symbol-to-phase mapping is inherently differential, [4]. So, in selected baseband differential detection, which is actually a coherent demodulation technique, the following observation variables x_k and y_k are extracted from the downconverted incoming signal:

$$x_k = \cos(\theta_k - \theta_0) \tag{2. 22}$$

$$y_k = \sin(\theta_k - \theta_0) \tag{2. 23}$$

where θ_k is the absolute phase of the incoming signal at sampling instants and θ_0 is the initial phase of the signal. The detection device operates using the observation variables formulated above, [15]. The outputs of the detection device, w_k and z_k, contain the phase difference between the two sampling instants as given below:

$$w_k = x_k x_{k-1} + y_k y_{k-1} = \cos(\theta_k - \theta_{k-1}) \tag{2. 24}$$

$$z_k = y_k x_{k-1} + x_k y_{k-1} = \sin(\theta_k - \theta_{k-1}) \tag{2. 25}$$

$(\theta_k - \theta_{k-1})$ quantity could take values in the set $\{\pm \pi/4, \pm 3\pi/4\}$, hence w_k and z_k could be $\pm 1/\sqrt{2}$. Hence, for the in-phase recovered data, the receiver decides in favor of symbol 1 if $w_k>0$, else symbol 0. Similarly, a symbol 1 is decided only if $z_k>0$, otherwise symbol 0 is recovered for the quadrature channel, [15].

The bit error ratio for differential detection of π/4-QPSK is examined with long calculations and approximations, and formulated as, [16]:

$$P_b = \frac{1}{2}\operatorname{erfc}\left(\sqrt{(2-\sqrt{2}) \times \frac{E_b}{N_0}}\right) \tag{2. 26}$$

2.6 Comparative BER Performances of PSK Modulation Schemes and Conclusion

Figure 2.11 demonstrates exact analytical bit error ratio, BER vs. E_b/N_0, curves for BPSK/QPSK/OQPSK, [12] and π/4-QPSK, [2]. These are given in solid lines where corresponding bit error probabilities for BPSK, QPSK and OQPSK are same. Also, the BER curve obtained with the described demodulator architecture in Section 2.5.2 for π/4-QPSK is shown by dashed line. Hence, theoretical performance of π/4-QPSK is 2.3 dB worse than that of other three schemes whose BER vs. E_b/N_0 characteristics are same.

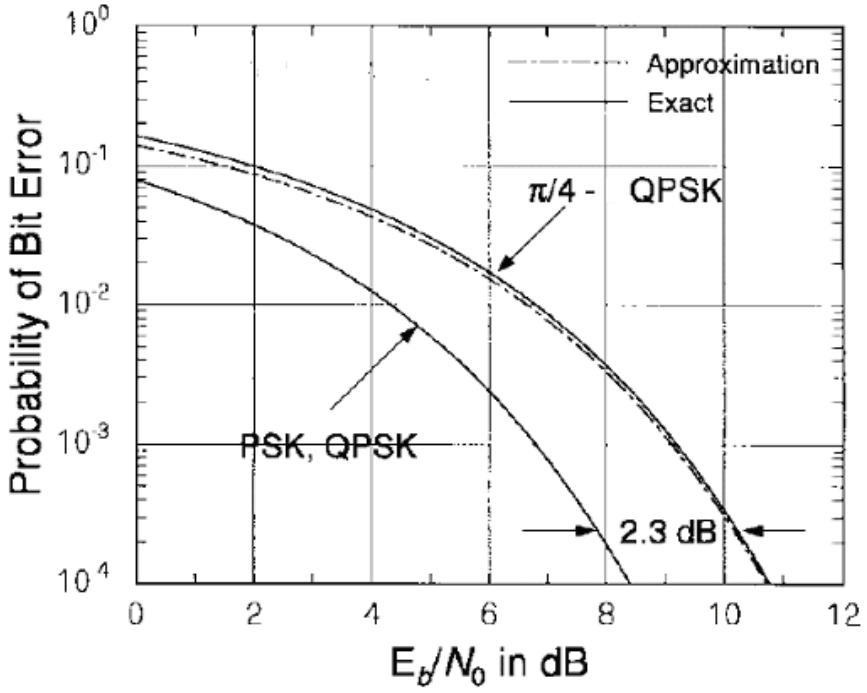

Figure 2.11 Exact and approximate bit error probability for π/4-QPSK with those of BPSK, QPSK, OQPSK, [16].

CHAPTER 3

MODELING OF NONLINEAR SYSTEMS FOR SIMULATION AND MODELING OF THE HIGH POWER AMPLIFIER DESIGNED AT BILTEN

3.1 Introduction

Study of all practical systems causes engineers to lean on modeling techniques in their works. This is necessary for determining the performance of linear systems by analytical means. But, the study of nonlinear systems is complicated, requiring additional tools than precise analytical modeling concept. The greatest justification for the simulation approach to the study of systems — in our case, communication systems — is obviously this necessity.

The nonlinear elements in a system, which are normally relatively few in number, are described by nonlinear functions or nonlinear differential equations relating the input and output of the element. The nonlinear part of the system has to be simulated in the time domain since superposition does not hold as in some transform methods, [4]. But, the rest of the system can be simulated either in the time domain or in the frequency domain.

The following section will introduce basic model-type descriptions for the amplifier nonlinearity phenomenon. A commonly used nonlinearity modeling technique in literature, namely memoryless baseband nonlinearity concept, will be clarified in Section 3.3. Then, Section 3.4 introduces probable empirically based memoryless bandpass amplifier models in scope. Section 3.5 describes the technique that is used

for measuring the solid state power amplifier (SSPA) characteristics with results and introduces the X-Band High Power amplifier (HPA) designed at TÜBİTAK-BİLTEN. In the final section, a brief discussion is made on nonlinearity models with memory for completeness.

3.2 Basic Model-Type Descriptions, [4]

Primary nonlinearity models can be classified as

- memoryless models
- models with memory

with each being either

- bandpass type, or
- baseband type

The most significant distinction is between a memoryless nonlinearity model and one with memory. The term ‘memoryless’ implies that output of a device is a function of the input signal at the present instant and transfer characteristic is frequency independent. Memoryless models are valid under the condition that the input signal has a bandwidth sufficiently smaller than that of the device. In fact, no physical device is truly input-frequency independent. Rather, as the bandwidth of an input signal increases, we can expect filtering effects to be manifested gradually. But, models with memory are considerably more difficult to obtain and more computationally demanding.

The term ‘bandpass model’ implies one that connects directly the complex envelopes of the input and output carriers. This is the type of model required if the purpose of the simulation is to extract a performance estimate. The term ‘baseband model’ implies that the input signal’s energy is concentrated around zero frequency and the nonlinearity’s output is also observed in that general vicinity.

3.3 Memoryless Nonlinearities: General Considerations, [4]

Memoryless nonlinearities are characterized in two general classes as baseband or bandpass types.

The model for a memoryless baseband nonlinearity is indicated by a simple functional relationship of the form

$$y(t) = F\left[x(t)\right] \tag{3. 1}$$

Such a relationship is used for most solid-state devices such as a simple diode volt-ampere characteristic.

Discussions suggest that the function F might be representable by a power series, an orthogonal function expansion or approximated over the range of $x(t)$ by a polynomial in x. For ease of modeling, the last one can be assumed and (3.1) can be expanded as

$$y(t) = F\left[x(t)\right] \approx \sum_{n=0}^{N} a_n x^n(t) \tag{3. 2}$$

where the coefficients a_n are obtained by fitting a polynomial of order N to a measured characteristic.

3.4 Memoryless Bandpass Amplifiers as Nonlinear Systems: Emprically Based Models for Simulation, [4]

Bandpass amplifiers constitute a huge example area for memoryless bandpass nonlinearities. Here, although only bandpass inputs can produce any measurable output, — the desired signal around the original carrier frequency — spurious signals (harmonics) are also produced. Practical-world measurements form a basis for almost all of the models that will be discussed for bandpass amplifiers.

It is a strong experimental observation that an input

$$x(t) = A\cos(2\pi f_c t + \theta) \tag{3. 3}$$

into a bandpass amplifier produces an output of the form

$$y(t) = g(A)\cos\left[2\pi f_c t + \theta + \Phi(A)\right] \tag{3. 4}$$

where gain function $g(A)$ is conventionally referred to as the AM/AM characteristic and the phase function $\Phi(A)$ is called the AM/PM characteristic. Hence, AM/AM conversion refers to a nonlinear relationship between input and output amplitudes and related distortion is quantified by various compression points[1]. AM/PM conversion refers to how the input amplitude affects the phase of the transmitted carrier.

Equation 3.4 can be extended such that the data signal bandwidth is nonzero, i.e., $A \rightarrow A(t)$, and also phase is time-varying, i.e., $\theta \rightarrow \theta(t)$. As indicated, if the bandwidth under concern is relatively small compared to the inherent bandwidth of the device, this assumption would be verified, so that if

$$x(t) = A(t)\cos\left[2\pi f_c t + \theta(t)\right] \tag{3. 5}$$

then

$$y(t) = g\left[A(t)\right]\cos\left\{2\pi f_c t + \theta(t) + \Phi\left[A(t)\right]\right\} \tag{3. 6}$$

Definition/Measurement of AM/AM and AM/PM characteristic curves is not unique. But, as long as memoryless assumption is accepted, the model introduced by (3.6) applies, no matter how the specific AM/AM and AM/PM curves are obtained.

Figure 3.1a is a symbolic block diagram of (3.6) at the carrier frequency level and Figure 3.1b is a simulation block diagram showing explicitly what must be done to implement the model.

---

[1] In RF circuits, this effect is quantified by the "1-dB compression point" (P_{1dB}), defined as the input signal level that causes the small-signal gain to drop by 1 dB. Also, the corruption of signals due to third-order intermodulation of two nearby interferers is so common and so critical that a performance metric, namely "third intercept point" (IP_3), has been defined to characterize this behaviour.

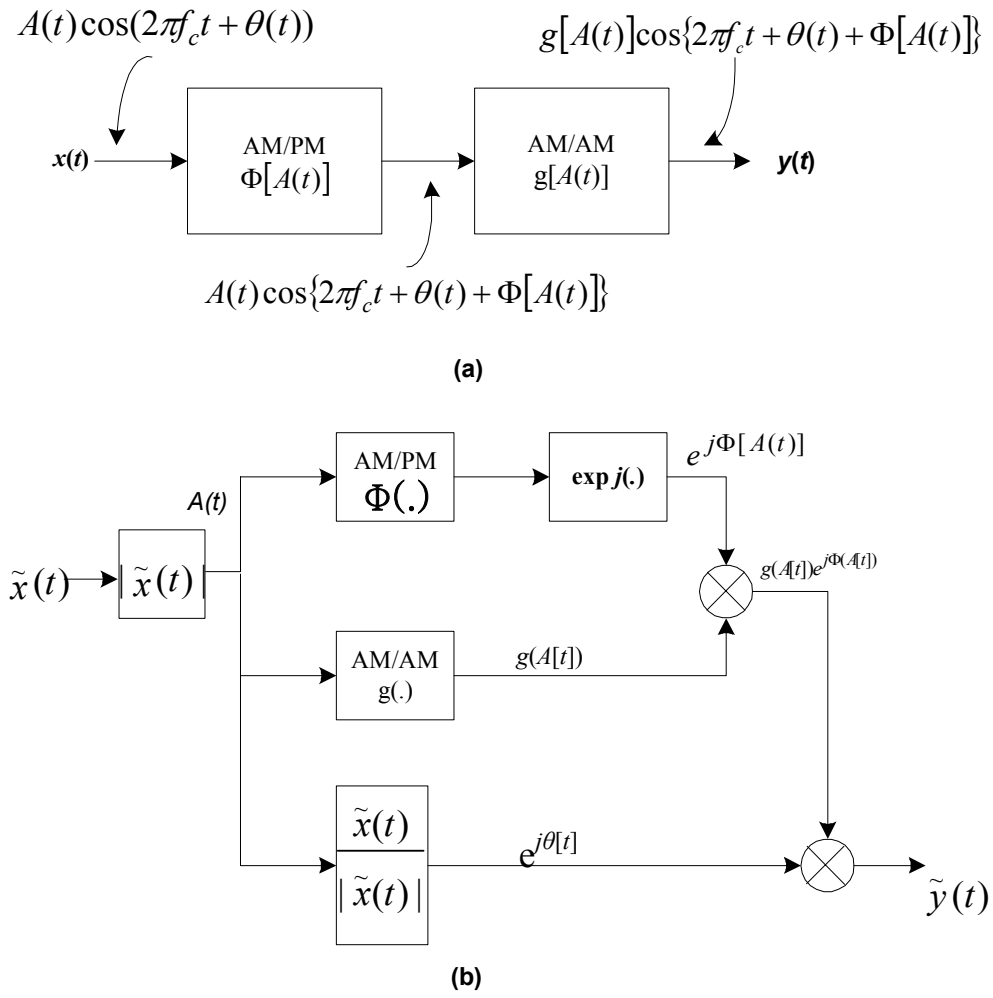

Figure 3.1 (a) Symbolic model at the carrier frequency level (b) explicit simulation model at the complex envelope level.

In this figure, $\tilde{x}(t)$ denotes the complex envelope of input waveform *x(t)* and $\left|\tilde{x}(t)\right|$ denotes its magnitude.

Also in literature, [5], [6], AM/AM and AM/PM conversion phenomena for various memoryless bandpass amplifiers are empirically based on two main models, which are introduced in the following two sections.

3.4.1 Saleh Model

In literature for memoryless bandpass traveling wave tube amplifiers (TWTA), [5], Saleh proposed the following forms for $g(A)$ and $\Phi(A)$:

AM/AM conversion: $$g(A) = \frac{\alpha_g A}{1 + \beta_g A^2} \tag{3. 7}$$

and

AM/PM conversion: $$\Phi(A) = \frac{\alpha_\Phi A^2}{1 + \beta_\Phi A^2} \tag{3. 8}$$

where A constitutes magnitude of the complex envelope of time domain signal and α_g, β_g, α_Φ, β_Φ are constants. This model offers a computationally efficient type of fitting-function set. Additionally, coefficients in (3.7)-(3.8) are determined by a least-squares fit. Figure 3.2 gives an example of normalized TWTA amplitude and phase data, where Saleh model approximation for these data is also shown.

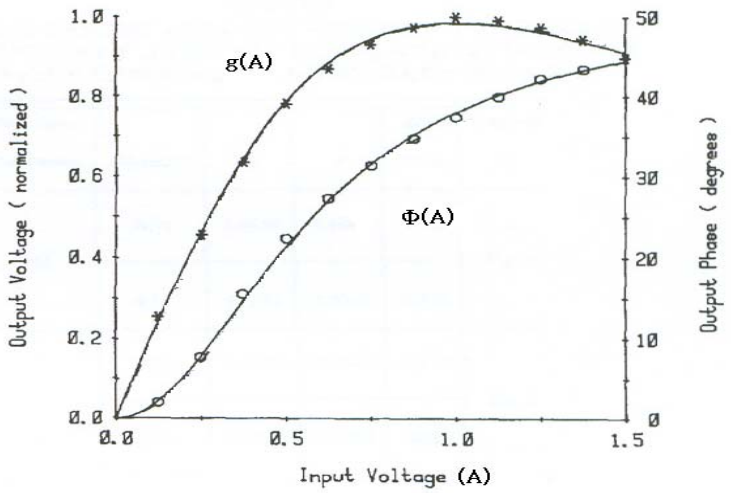

Figure 3.2 Example for TWTA amplitude (*) and phase (o) data, [5]. The solid lines are from (3. 7) and (3. 8).

As can be understood from the given figure, increasing the input voltage causes a nonlinear increase in both AM/AM and AM/PM conversion curves. Interesting point in AM/AM conversion curve of Saleh model is that output voltage tends to decrease from a point on.

3.4.2 Rapp Model

In the literature, memoryless bandpass solid state power amplifiers (SSPA) are modeled mathematically by a widely accepted model, namely, Rapp Model, [6], encompassing amplitude clipping and phase distortion. Here, amplified signal and amplifier gain can be expressed as

$$u(t) = s(t)G[|s(t)|] \tag{3.9}$$

$$G[|s(t)|] = \frac{A[|s(t)|]e^{j\Phi[|s(t)|]}}{|s(t)|} \tag{3.10}$$

with the following related nonlinear transformations

AM/AM conversion:
$$A[|s(t)|] = \frac{K_1|s(t)|}{\left[1+\left(\frac{K_1|s(t)|}{A_0}\right)^{2p}\right]^{\frac{1}{2p}}} \tag{3.11}$$

AM/PM conversion:
$$\Phi[|s(t)|] = \alpha_\varphi\left(\frac{K_1|s(t)|}{A_0}\right)^4 \tag{3.12}$$

where A_0 is the saturating amplitude, K_1 is the small signal gain, $s(t)$ is the complex envelope of the input signal, p is a parameter which controls the smoothness of the transition from the linear region to the saturation region. α_φ is typically set to zero, meaning SSPA adds no phase distortion, [6]. Hence, a normalized AM/AM conversion characteristic example is given in Figure 3.3.

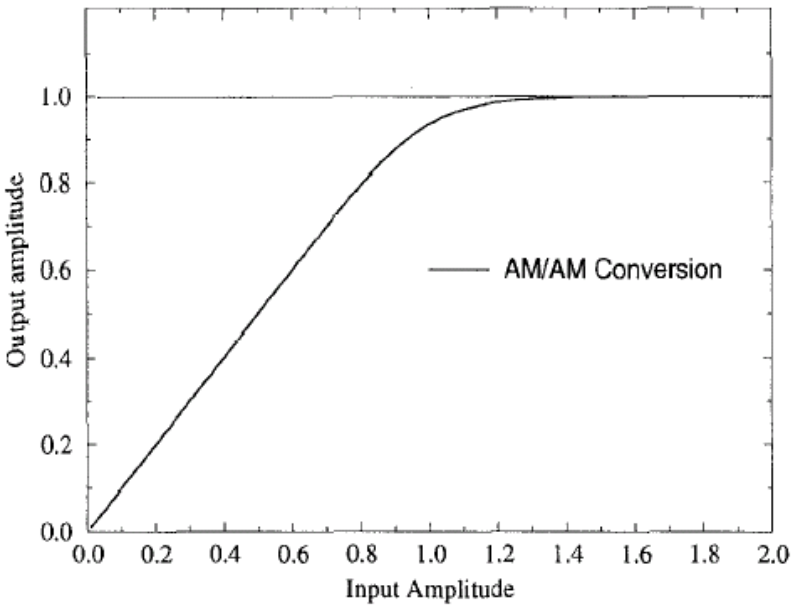

Figure 3.3 SSPA characteristic of Rapp Model with normalized AM/AM conversion, [6]

In this figure, in contrast to AM/AM conversion curve of the Saleh model, curve settles at a value which indicates a fixed voltage output.

3.5 The High Power Amplifier and Characterization Technique

The block diagram of the SSPA to be characterized is given in Figure 3.4. This is a cascaded narrowband three-stage power amplifier. First stage is a linear driver amplifier manufactured by MITEQ Cooperation. Last two stages are in scope and are designed at TÜBİTAK-BİLTEN to have a total power gain of 21.6 dB and output power of 38.5 dBm at 8.2 GHz with a bandwidth of 95 MHz as operating conditions (Gain flatness is ± 0.6 dB in 8.17-8.265 GHz band).

Since HPA will deal with narrowband input signals having a bandwidth sufficiently smaller than that of the device, it can be modeled as a memoryless device, [4]. Moreover, considered HPA is solid state transistor based, therefore the Rapp model is chosen for characterization, [6]. As discussed in the previous section, this model stipulates no phase distortion. Hence, only magnitude distortion (see (3.11)), i.e., AM/AM distortion, will be considered for characterization.

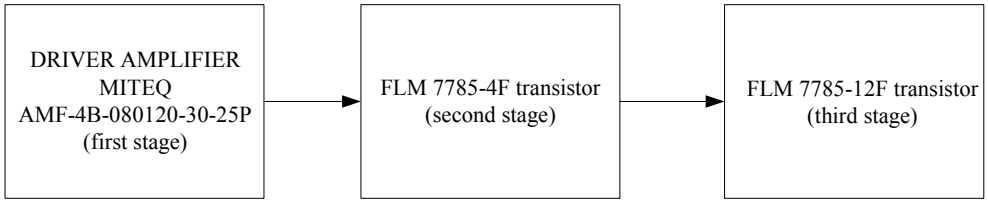

Figure 3.4 The HPA block diagram

Since the single tone measurement is the most widely accepted technique in laboratories, [4], it is adopted to measure the forward transmission response (S_{21}). This test is accomplished under the usual working conditions[2] of the HPA, [17]. Figure 3.5 demonstrates the test setup for the characterization.

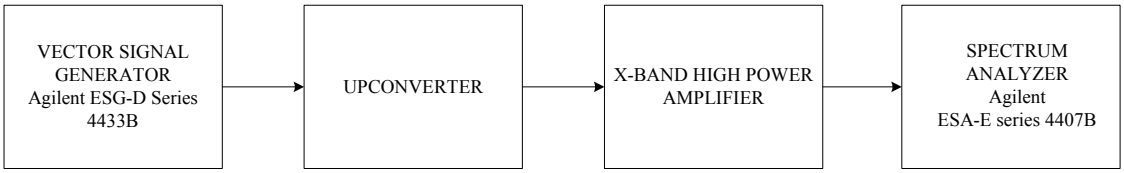

Figure 3.5 Test setup

In this process, the single tone stimulus at the center operating frequency (8.2 GHz) is introduced to HPA to cover the dynamic range of interest. The values measured are given in Table 3.1.

[2] Drain voltages of transistors belonging to both stages are 9 V. Gate voltage of the first stage transistor is -0.5 V whereas that of second is –1.1 V.

Table 3.1 Power input to last two stages and overall PA output

Power input to last two stages (dBm)	Overall PA output (dBm)
12.2	**33.8**
15.2	**36.8**
16.2	**37.8**
17.2	**38.8**
18.2	**39.6**
19.3	**40.2**
20.3	**40.6**
21.4	**40.8**
22.4	**41**
23.4	**41.1**
24.3	**41.1**

Since the spectrum analyzer in the test setup measures the power of the output signal, time domain Rapp model equation should be adapted to process power values. Hence considering (3.11), average input power and average output power are respectively, [4]

$$P_{in} = \frac{[A(|s(t)|)]^2}{2} \qquad P_{out} = \frac{[G(|s(t)|)]^2}{2} \tag{3. 13}$$

In connection, extraction of Rapp model parameters ─ A_0 and K_1 ─ from data in Table 3.1 can be clarified as follows. Saturating overall PA output power ($A_{0,power}$) is read to be 41.1 dBm from Table 3.1 and is connected to A_0 as

$$A_0 = \sqrt{2A_{0,power}} \tag{3. 14}$$

K_1 is the small-signal gain, that is, it gives the uncompressed voltage gain of the amplifier block. Since first four couple of entries of Table 3.1 demonstrate no gain compression ─ that is difference between output and input power levels are same for these entries, *i.e.*, 21.6 dBm ─ any of these entries can be used to calculate the uncompressed power gain ($K_{1,power}$) where

$$K_1 = \sqrt{2K_{1,power}} \tag{3. 15}$$

After finding A_0 and K_1, there only remains smoothness factor p which should be determined through an optimization process. To fit the measured results into parametric descriptors of the selected power amplifier nonlinear model, Least Squares (LS) Fitting Method, [18], is selected. It is a mathematical procedure for finding the best-fitting curve in mean square error sense to a given set of points by minimizing the sum of the squares of the offsets (residuals) of the points from the curve according to

$$R^2 = \sum \left[y_i - f\left(x_i, a_1, a_2, ..., a_n\right) \right]^2 \tag{3. 16}$$

where y_i values denote the given set of points, $f(x)$ denotes estimating curve with a_i to be optimized and R^2 is the result to be minimized with respect to a_i.

If y_i values are selected according to PA output (see Table 3.1), $f(x)$ is selected to be the Rapp model AM/AM conversion function with determined parameters $a_1=K_1$, $a_2=A_0$, and optimization parameter is assumed to be p, the result of optimization turns out to be $p = 3.8$.

Figure 3.6 gives both the calculated parameter values and obtained characteristic in a graphical manner. High consistency with the measured values is observed, which verifies the selection of Rapp model and the modeling process.

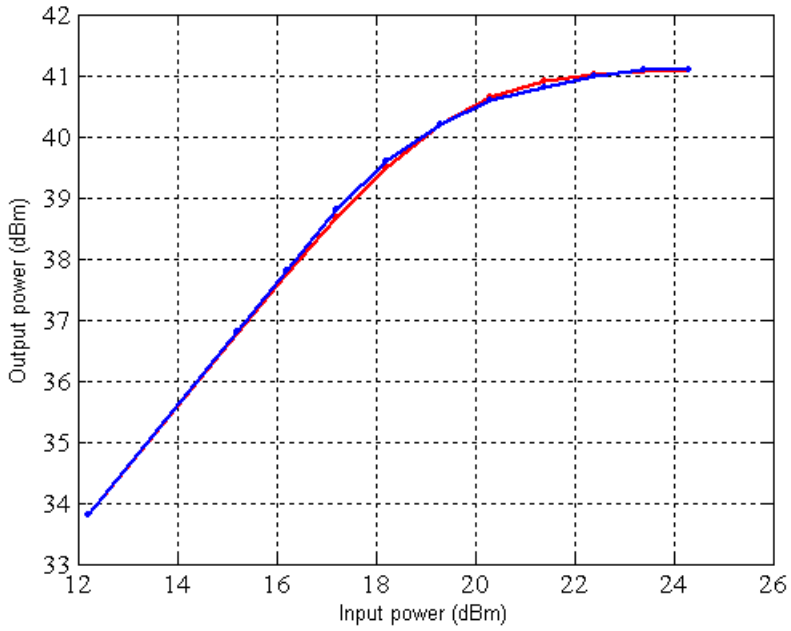

Figure 3.6 Measured (Blue) and Rapp modeled amplifier characteristics with K_1=17, A_0=160.5, p=3.8 (red)

3.6 Nonlinearities with Memory: General Considerations, [4]

Although nonlinearities with memory are not considered in this study, general considerations are preferred to be summarized for the sake of completeness. A nonlinearity with memory can be defined as one whose output depends on a segment (finite or infinite) of the input signal prior to measurement time t for causality. Memory implies a filtering effect caused by the frequency dependent nonlinear characteristics. Considering nonlinearity models with memory, it is useful to define three broad classes of characterization: macroscopic, microscopic, and analytical models.

By macroscopic models, those constructed on the basis of input/output measurements using an appropriate probing signal are meant. The nonlinear system is considered as a black box, using measurement techniques to "identify" a topology. The drawback of such models is their variable accuracy, nevertheless, they constitute the standard approach for system-level simulation for nonlinearities with memory.

By microscopic models, those which are exact at the intended level of representation are meant. In this approach, some degree of internal access to the model is obtained.

The third general modeling category is analytical representation, for example, Volterra series are able to represent exactly the functioning of some nonlinear blocks with memory. In a sense, such models stand at the intersection of previous two modeling understanding.

CHAPTER 4

PERFORMANCE CRITERIA

4.1 Introduction

Simulation of communication systems requires lots of care on issues to be tackled. In this chapter, the methodology used in simulating distortion effects on four PSK type modulation schemes ─ summarized in Chapter 2 ─ is introduced.

Being a strong engineering software tool, MATLAB® (version 6.5) is chosen as the simulation environment. It is an easily-reached software that owns a huge number of embedded telecommunication-related functions. These functions comfort either to build up basic interconnected communication blocks or to catch the main ideas in telecommunication theory by simplifying software scripts. Communication line-up that is implemented in MATLAB® is thoroughly given in Section 4.2. Power amplifier model characteristic utilized for simulations is explained in Section 4.3.

In Section 4.4, performance evaluation parameters under nonlinearity for PSK type modulation schemes are considered. In Section 4.4.1, two types of bit error rate (BER) estimates are given. The first one is based on a simple counting argument and it is commonly used. However, since it is not appropriate for very high signal to noise ratio (SNR) values due to time limitation in simulation, the second BER estimate is introduced in this study. In Section 4.4.2, error vector magnitude (EVM) concept, [19], is given, which is a good transmitter performance evaluation parameter. In Section 4.4.3, Space Frequency Coordination Group (SFCG) 21-2

spectral mask constraint is given. This parameter, also, constitutes important limiting criteria in both global system for mobile communications (GSM) and space communications, [20]. In Section 4.5, optimum parameter for the matched filters for each modulation scheme is found. Finally, in Section 4.6, complementary cumulative distribution function (CCDF) is defined to discuss the simulation results.

4.2 Program Structures on MATLAB

Communication transmit/receive line-up that is implemented in MATLAB® for all modulation schemes is shown in Figure 4.1.

The most important characteristic of communication line-up used for simulation is its complex envelope characterization, i.e., it replaces sinusoidal carrier signals in the modulator block of PSK-type signaling with complex number representation, [4]. It also utilizes no frequency upconversion block as a result of nonlinear block modeling described in Chapter 3. The mentioned method constitutes the main strategical steps in creating a non-time-consuming simulation environment in computer, where high sampling rate should be used to capture nonlinearity effects, [4].

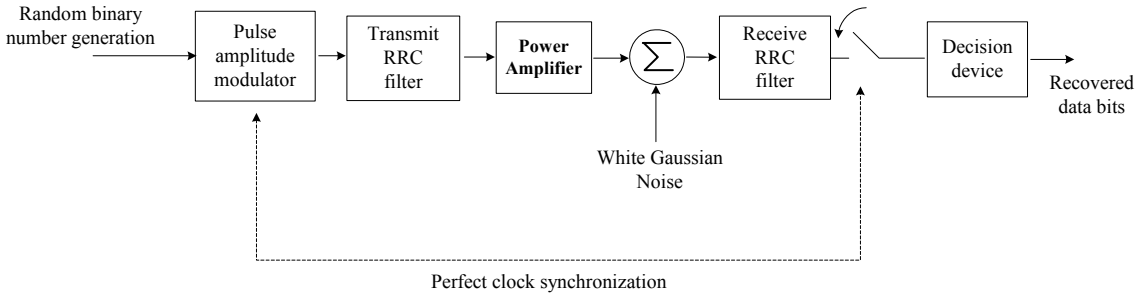

Figure 4.1 Communication transmit/receive line-up

At the input of the line-up, random binary numbers are generated as input bits (1's and 0's) to modulator block, which transforms this binary sequence into a new sequence of unit polar (±1) impulses, [12], and additionally, applies modulation process according to the selected PSK scheme. Then, root raised cosine (RRC)

filtered signal (see Appendix A) is applied to the PA block, where it experiences parameterized AM/AM nonlinearity.

Channel is modeled as an AWGN channel, which is frequently used in the literature, [12]. At the receiver side, again, an RRC type filter is used that is matched to RRC transmit filter. Though PA distorts the matched property of transmit/receive filters, the receiver structure does not include an extra block for the compensation of this mechanism which is also the case in the real world application. Since device under simulation introduces no phase distortion (see section 3.4), sampling device uses the same clock instants with that of the transmitter. Finally, bits in error are determined with a detection device and performance estimates are calculated.

4.3 Power Amplifier Model Utilized for Simulations

In Chapter 3, modeling of the X-Band High Power amplifier (HPA) designed at TÜBİTAK-BİLTEN is introduced, where smoothness factor parameter p is found to be p=3.8 for a special case. But, for simulation purposes, two p values are selected as p=0.8 and p=5. This gives an opportunity to evaluate the effect of p at operating points close to upper and lower limits of this parameter. Meanwhile, linear region power gain and saturating power amplitude are fixed respectively as 0 dB and 0 dBm (see Figure 4.2), which corresponds to A_0=1 and K_1=1 case (see Section 3). The reason is that variation of these parameters will not be investigated throughout the study.

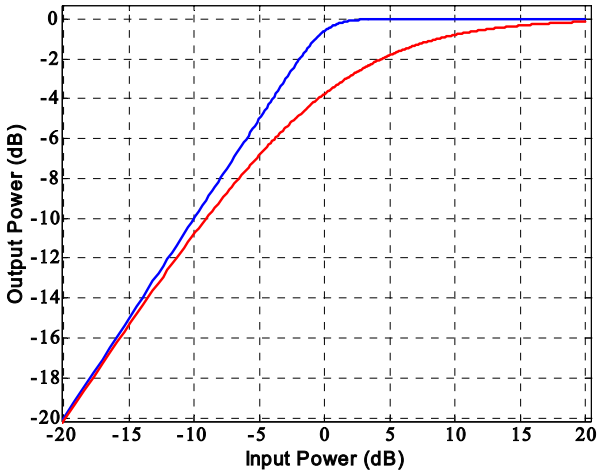

Figure 4.2 Simulation PA curves with varying p values, red: p=0.8, blue: p=5

As can be understood from the figure, variation of p affects the smoothness of the transition from the linear region to the saturation region in the PA characteristic.

4.4 Performance Evaluation Parameters under Nonlinearity

4.4.1 BER Estimates at the Receiver Side

The most definitive figure of merit to assess the noise performance of communication systems has been the average probability of symbol error (SER). However, when the requirement is to transmit binary data, it is often more meaningful to use another figure of merit called bit error ratio (BER), [12] (Interrelation between these two quantities is clarified when Gray encoding is discussed in Chapter 2). Bit error probability results are also summarized in terms of E_b/N_0 for related modulation schemes in Chapter 2 for theoretical completeness, though are not used in this given form throughout the study.

Hence, in simulations for low SNR=E_b/N_0 values, a simple counting argument is used for determination of BER estimate as

$$\hat{\mathrm{BER}} = \frac{\text{number of received erroneous bits}}{\text{number of total transmitted bits}} \qquad (4.1)$$

However, BER estimate calculation described above is quite time-consuming for high E_b/N_0 values in simulation process. Therefore, the mean and the variance of sample points at the receiver end are determined by Monte Carlo method, [4], and are used in bit error probability 'P_b' estimate. This estimate calculation is realized for all PSK modulation schemes other than π/4-QPSK. The resultant expressions for P_b are given in the following two sections; the details can be found in Appendix B.

4.4.1.1 BPSK/QPSK/OQPSK Bit Error Probability Calculation

BPSK bit error probability calculation results in the following equation (see Appendix B.1):

$$P_b \cong \text{BER} = 1 - \frac{1}{2}\text{erfc}\left(\frac{-\mu_x}{\sqrt{2}\sigma_x}\right) \tag{4. 2}$$

where μ_x is the mean of the sample points, σ_x is the standard deviation of the sample points' distribution and erfc is the complementary error function defined as

$$\text{erfc}(x) = \frac{2}{\sqrt{\pi}}\int_x^\infty e^{-t^2}\,dt \tag{4. 3}$$

QPSK/OQPSK bit error probability can be expressed in terms of a known mathematical function, if we utilize Gray encoding (see Section 2.3.1) for the data bits as follows:

$$P_b \cong \text{BER} = \frac{1}{2}\left(1 - \frac{1}{4}\text{erfc}\left(\frac{-\mu_x}{\sqrt{2}\sigma_x}\right)\text{erfc}\left(\frac{-\mu_y}{\sqrt{2}\sigma_y}\right)\right) \tag{4. 4}$$

P_b for OQPSK is same as that of QPSK.

4.4.2 Error Vector Magnitude, [19]

The error vector represents the difference between the measured signal and a reference (a perfectly demodulated signal) as illustrated in Figure 4.3 and EVM is the magnitude of the error vector as given below

$$EVM = \sqrt{(I_{MEAS} - I_{REF})^2 + (Q_{MEAS} - Q_{REF})^2} \qquad (4.5)$$

where I_{MEAS} and Q_{MEAS} are the quadrature components of the measured signal, and I_{REF} and Q_{REF} are the quadrature components of the reference signal. This quantity is expressed in percentage as normalised to the reference signal magnitude.

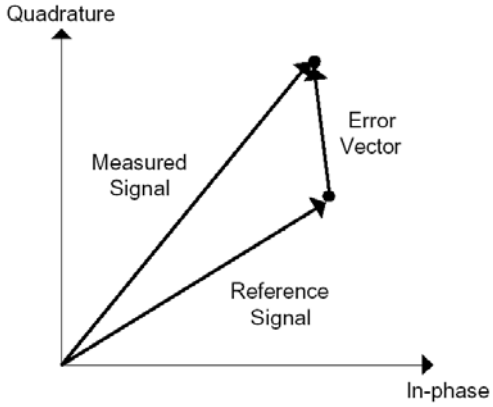

Figure 4.3 The error vector

4.4.3 Spectral Mask Concept and Imposed Constraint by SFCG 21-2 in Space Communications

In space communications as well as in terrestrial communications (e.g., GSM), optimum spectrum utilization has resulted in channels that are very close or slightly overlapped. A certain amount of signal appears in the adjacent channels due to modulation limitations and/or because of channel overlap. In addition to this, there may be an increase in the relative distortion levels in the adjacent channels due to nonlinear amplification of a signal, [21].

Space Frequency Coordination Group (SFCG) is an institution which was established in order to provide a less formal and more flexible environment as compared to the official organs of the International Telecommunication Union (ITU), [22]. This institution strongly recommends, [23], a spectral mask for the spectra belonging to transmitters of spacecrafts' downlink communication units (Figure 4.4).

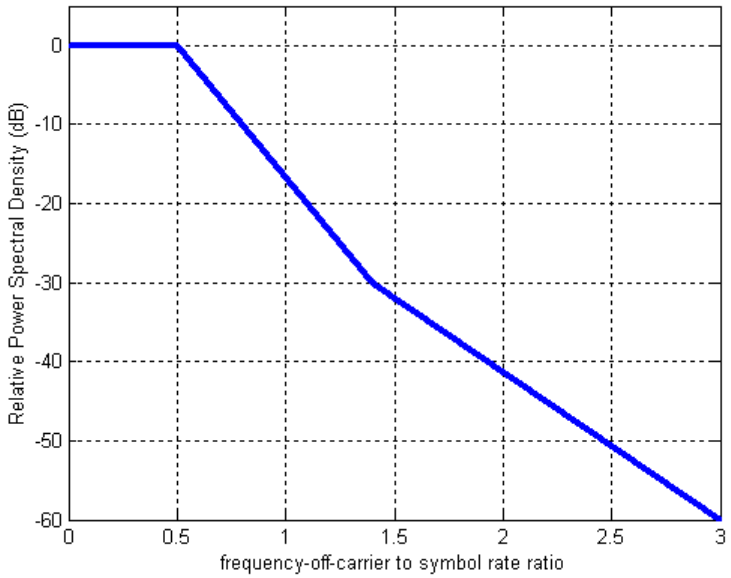

Figure 4.4 SFCG Rec.21-2 Spectral Mask

This figure gives the spectral mask as normalized to the maximum value of the signal spectra. Frequency axis nomenclature makes this definition unique for all modulation schemes.

In the simulations, the Welch spectral estimation method, [24], is also used to estimate the power spectral densities (PSD) of the PSK modulation schemes in scope and is detailed in Appendix C with the used methodology. In the next subsection the mathematical background of the relative increase in signal spectra observed in modulated and filtered (variable envelope) signals is given.

4.4.3.1 Spectral Regrowth in Variable Envelope Signals, [10]

Constant and variable envelope signals behave differently in a nonlinear system. If a variable envelope signal is considered as

$$x(t) = x_I(t)\cos\omega_c t - x_Q(t)\sin\omega_c t \tag{4. 6}$$

and is applied to a system (where $x_I(t)$ and $x_Q(t)$ are the baseband I and Q components) exhibiting, *e.g.*, a third-order memoryless nonlinearity (see Section 3.3), output will be

$$y(t) = a_3 x^3(t) \tag{4. 7}$$

$$= a_3 x_I^3(t)\frac{\cos 3\omega_c t + 3\cos\omega_c t}{4} + a_3 x_Q^3\frac{\cos 3\omega_c t - 3\sin\omega_c t}{4} + \text{cross terms} \tag{4. 8}$$

As seen, the output contains the spectra of $x_I^3(t)$ and $x_Q^3(t)$ centered around ω_c. Also, these components generally exhibit a broader spectrum than do $x_I(t)$ and $x_Q(t)$. As a result, not only spectrum grows but also an in-band distortion is seen when a variable-envelope signal passes through a nonlinear system.

Filtering a digitally modulated (*e.g.*, PSK-type) signal tends to smooth out the abrupt transitions in the time domain, but also causes the signal to exhibit variation in its envelope. If a block (*e.g.*, PA) exhibits significant nonlinearity, the shape of $x_I(t)$ and $x_Q(t)$ is not preserved and the spectrum is not limited to the desired bandwidth. This effect is called "spectral regrowth" in literature, [25], which is also accompanied by an in-band distortion.

4.5 Optimum Roll-off Value for Matched RRC filters under Nonlinearity

Modulation schemes show different BER performances against nonlinearity with different transmit-receive filter characteristics, [26]. For an RRC filter, the parameter that changes the characteristic turns out to be filter roll-off factor. Figures 4.5–4.8

clarify optimum roll-off values for four modulation schemes at E_b/N_o=11 dB for two different PA smoothness factors (p=0.8 and p=5). In these simulations, roll-off value is both for transmit and receive filters, which is the consequence of matched filtering property. Given graphical analysis is made for three main operating regions, namely, when PA operates in linear region, P_{1dB}, and in saturation region.

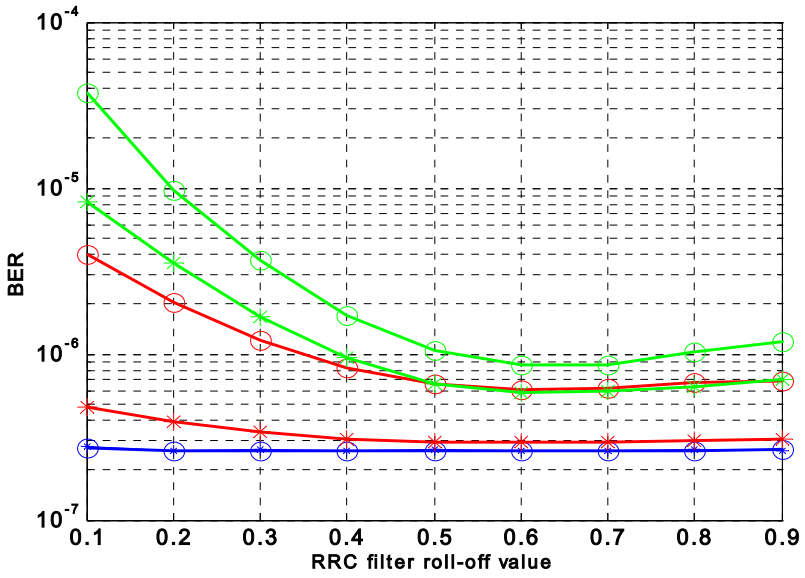

Figure 4.5 BER vs. RRC filter roll-off value for QPSK at E_b/N_o=11 dB at linear region (blue lines), P_{1dB} (red lines), saturation region (green lines). Marking with '*' indicates p=0.8, where 'o' indicates p=5.

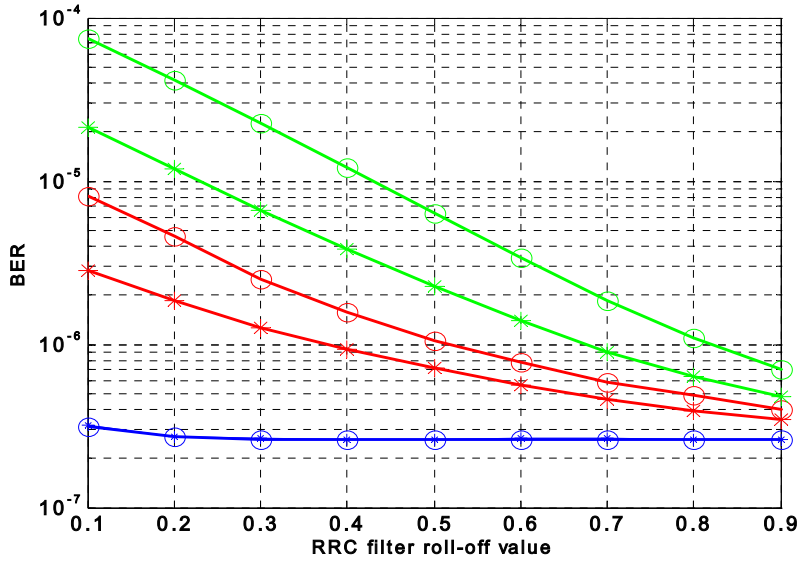

Figure 4.6 BER vs. RRC filter roll-off value for OQPSK at E_b/N_o=11 dB at linear region (blue lines), P_{1dB} (red lines), saturation region (green lines). Marking with '*' indicates p=0.8, where 'o' indicates p=5.

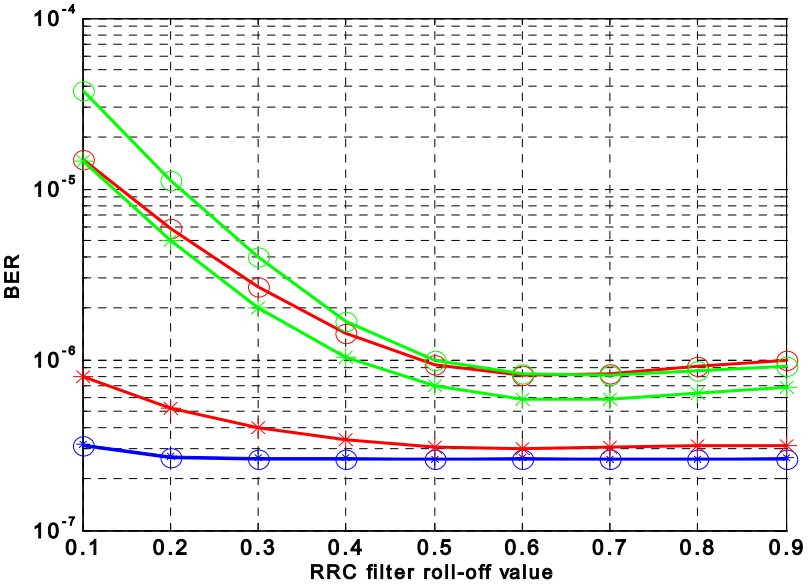

Figure 4.7 BER vs. RRC filter roll-off value for BPSK at E_b/N_o=11 dB at linear region (blue lines), P_{1dB} (red lines), saturation region (green lines). Marking with '*' indicates p=0.8, where 'o' indicates p=5.

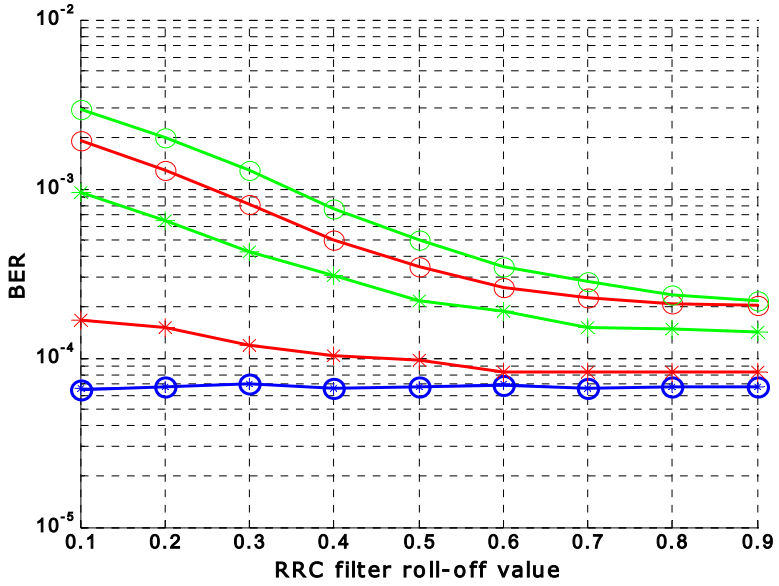

Figure 4.8 BER vs. RRC filter roll-off value for π/4-QPSK at E_b/N_o=11 dB at linear region (blue lines), P_{1dB} (red lines), saturation region (green lines). Marking with '*' indicates p=0.8, where 'o' indicates p=5.

From above plots, it can be inferred that in the linear region, RRC roll-off value does not have an effect on the BER performance, hence same BER for two different smoothness factor (p) values are observed. But, in P_{1dB} and saturation region operation of PA, simulation results in the plots clearly show that there exists an optimum pulse shaping parameter (RRC roll-off value) minimizing BER for BPSK and QPSK schemes. But, OQPSK and π/4-QPSK schemes behave in a different manner, showing an always-decreasing BER characteristic for increasing roll-off value under nonlinear operation. Clarification of this situation is so involved, but it may be related to the variation of Intersymbol Interference (ISI), [12], in the signal with varying roll-off factor. Then, optimum roll-off value is taken as 0.65 for completeness in all simulations, whereas 0.35 and 0.95 values are also considered as lower and upper practical limits.

4.6 Complementary Cumulative Distribution Function (CCDF) for Modulation Schemes, [27]

A CCDF curve shows how much time the signal spends at or above a given power level. The power level is expressed in decibels (dB) relative to the average power. Thus, the percentage of time the signal spends at or above a given power level defines the probability for that particular power level. A CCDF curve is a plot of relative power levels versus probability, where an example is given in Figure 4.9 below.

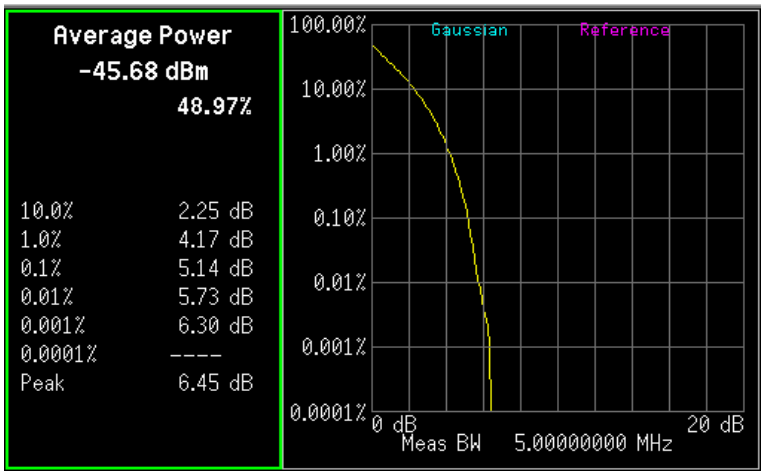

Figure 4.9 CCDF curve example for a 1 Megasample/sec (MSPS) QPSK signal with RRC filter rolloff factor α equals 0.

Traditionally, a common measure of stress for a stimulating signal has been voltage peak-to-average ratio (crest factor), [28]. This measure is of questionable value mainly because it places too much emphasis on a signal's instantaneous peak value while CCDF lessens this emphasis. CCDF gives us more complete information about the high signal levels than does crest factor.

We can also plot measured power CCDF curves of four modulation schemes at 1 MSPS data rate versus three different roll-off factors (α=0, 0.65, 1). Measurements are taken using Agilent 4430ESG-D signal generator and Agilent 4407B spectrum analyzer. Figures 4.10-4.12 give the results.

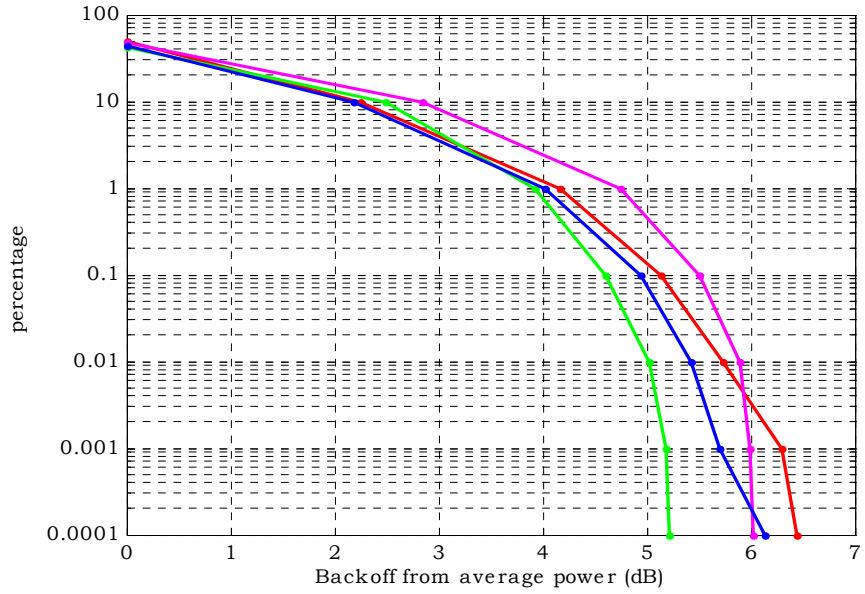

Figure 4.10 1 MSPS signals with RRC filter α=0, red: QPSK, blue: π/4-QPSK, green: OQPSK, magenta: BPSK

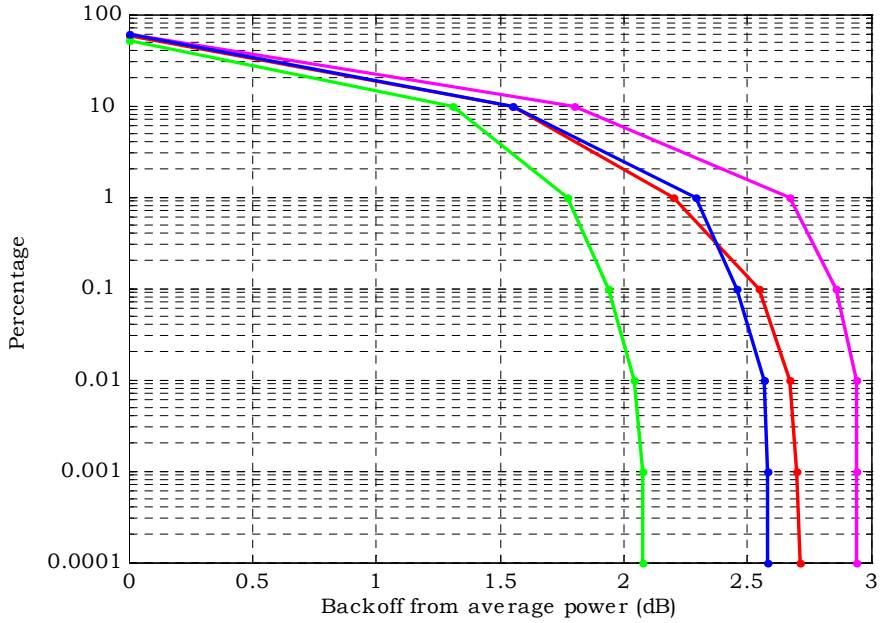

Figure 4.11 1 MSPS signals with RRC filter α=0.65, red: QPSK, blue: π/4-QPSK, green: OQPSK, magenta: BPSK

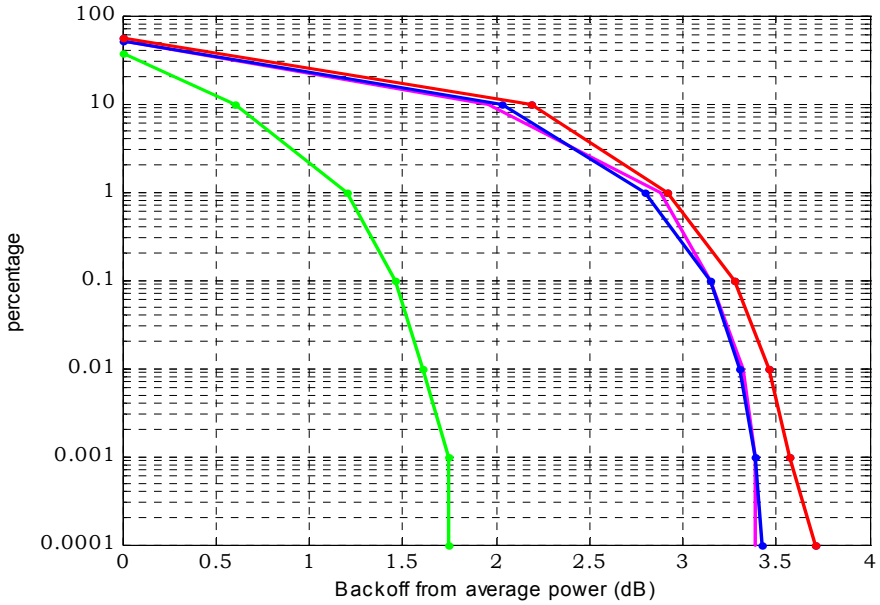

Figure 4.12 1 MSPS signals with RRC filter α=1, red: QPSK, blue: π/4-QPSK, green:OQPSK, magenta: BPSK

As seen from CCDF figures, quantities differ not only for each modulation scheme at a constant RRC filter roll-off factor, but also for different values of this filter parameter. It can be seen that curve characteristics tend to be similar for the modulation schemes investigated where OQPSK is an exception, dropping out of the general trend in these plots.

Also, taking three plots into account, maximum deviations from average power, generally, decrease with increasing roll-off value. But, BPSK, QPSK, and π/4-QPSK have minima in this case, where OQPSK does not.

These results will be used later for reasoning various phenomena and will be attributed in the next chapter.

CHAPTER 5

RESULTS AND DISCUSSIONS

5.1 Introduction

Nonlinearity effects are investigated on PSK-type modulation schemes (BPSK, QPSK, OQPSK, π/4-QPSK) with the use of simulations and results are given with the related discussions throughout this chapter. First, effects on transmitted constellation diagrams are given to clarify the situation of modulated sample points under nonlinearity for quadrature modulation schemes. Then, BER performances of all PSK-type schemes are given comparatively for two different values of the PA smoothness factor p, and for three different values of the RRC roll-off factor α. Lastly, spectral distortions on these four schemes are respectively examined in comparison with SFCG 21-1 Spectral Mask (explained in Section 4.4.3).

5.2 Nonlinearity Effects on Transmitted Constellation Diagrams of Quadrature Modulation Schemes

It is informing to see the effects of nonlinearity on the data carrying parts of the signal (sample points) for the digital modulation schemes. For this reason, investigation on the constellation diagrams of the signal types after nonlinearity is required. This will obviously, help to understand the nonlinearity affect at the first stage before the channel.

Following parts, consequently, will introduce the constellation diagram for three quadrature modulation schemes (QPSK, OQPSK, π/4-QPSK) before and after PA in

the transmitter side. Results of all three modulation schemes will be given only for α=0.35 ; p= 5 condition, while PA is operating at P_{1dB}. This condition is sufficient to carry out the anticipated discussions.

5.2.1 QPSK

RRC filtered signal's data sample points in the transmitter side are normalized in amplitude and given in Figure 5.1. Scattering of these sample points in fact indicates the variation of the signal's amplitude by filtering process.

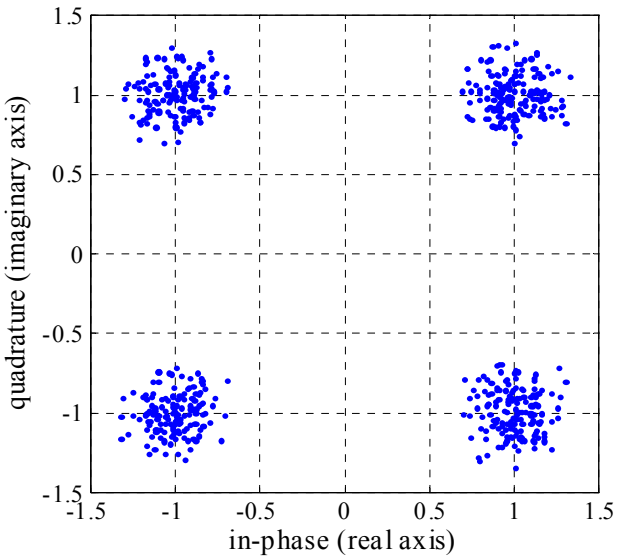

Figure 5.1 RRC filtered QPSK signal's data sample points for α=0.35

Figure 5.2 shows the situation of the sample points after the signal is exposed to PA operating at P_{1dB} with p=5. Again, sample points are normalized in amplitude.

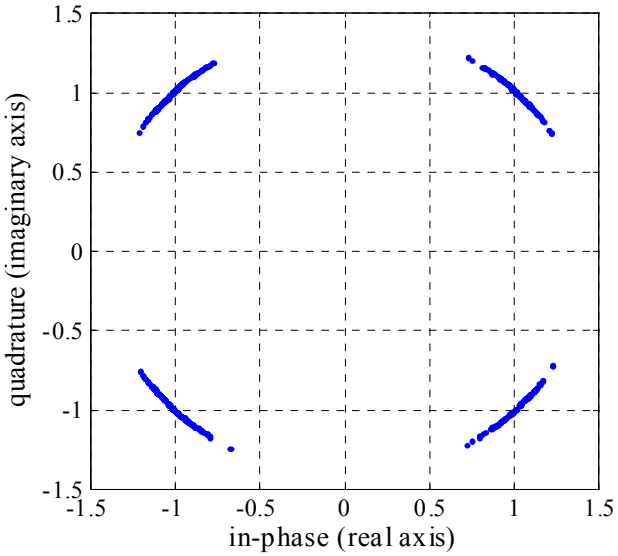

Figure 5.2 RRC filtered QPSK signal after PA operating at P_{1dB} with p=5

Since PA nonlinearity is modeled as affecting the complex envelope of the signal and in-phase/quadrature modulated data components in QPSK are carried by the same sample point, nonlinearity effect shows itself as circularization of constellation diagram. When this signal experiences the communication channel and is then demodulated, an increase in error rates is naturally anticipated.

5.2.2 OQPSK

When the same discussion is carried out for OQPSK case, it can be seen that, first, the same kind of constellation diagram is reached with that of QPSK in Figure 5.1. But, modulation mentality difference between these two schemes (see Section 2.4) shows itself when OQPSK modulated signal faces nonlinearity. The corresponding normalized constellation diagram is shown in Figure 5.3.

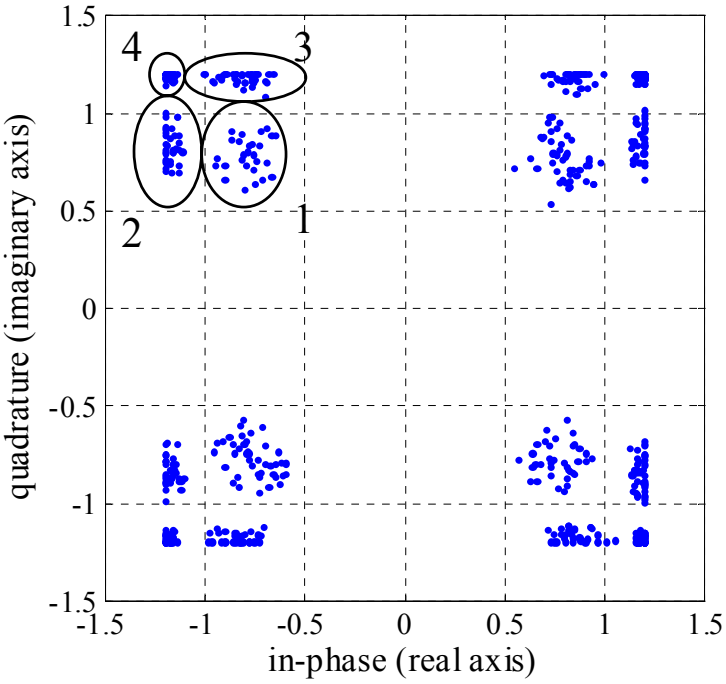

Figure 5.3 RRC filtered OQPSK signal after PA operating at P_{1dB} with p=5

Since, in OQPSK, in-phase and quadrature data points are not carried at the same sample point in the envelope, these data points are, relatively, affected independently from nonlinearity. Hence, accumulation at four main areas can be observed, instead of circularization: '4' indicates the accumulation area where both in-phase and quadrature modulated sample points are at the edge of saturation, '2' and '3' indicate the accumulation areas where one of them is saturated and finally '1' indicates the accumulation area where neither of them are saturated. Vulnerability of OQPSK modulation to nonlinearity is different from that of QPSK, and these will be clarified in the following sections.

5.2.3 Π/4-QPSK

Π/4-QPSK's constellation diagram has 8 points (as explained in Section 2.5) and that of RRC filtered signal is given in Figure 5.4.

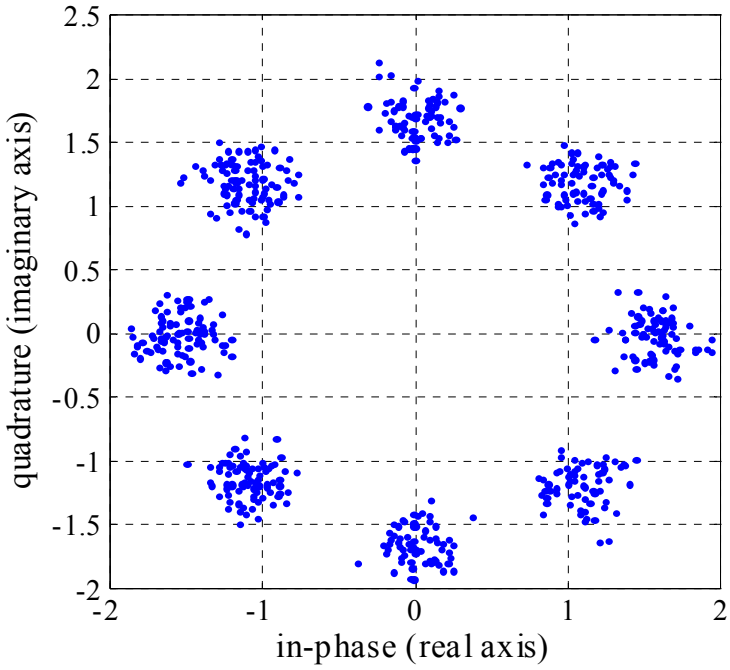

Figure 5.4 RRC filtered π/4-QPSK signal's data sample points for α=0.35

Modulation mentality does not differ from that of QPSK, so also in π/4-QPSK case nonlinearity effect shows itself as circularization of constellation diagram as given in Figure 5.5. Effects of these distortions on the BER performances of nonlinearly processed PSK signals can be mitigated to an extent by error correction coding, [2].

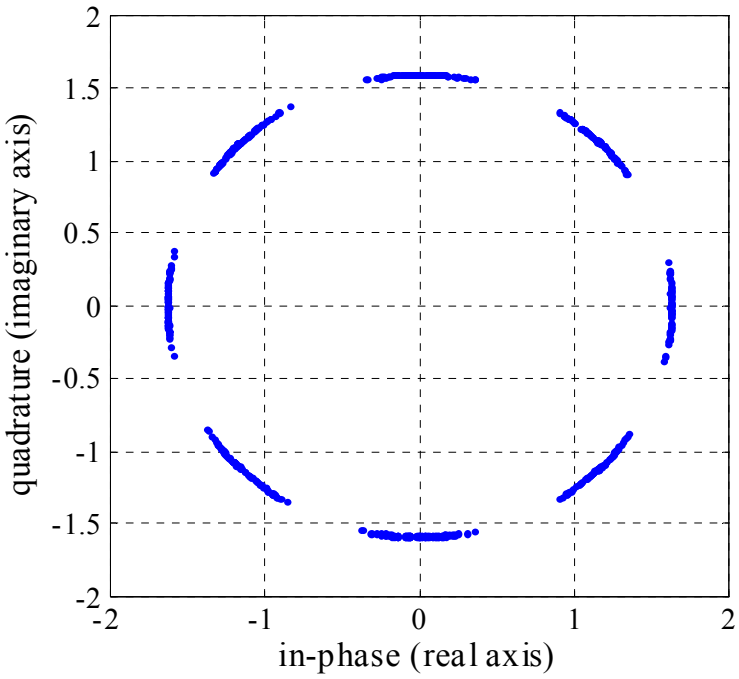

Figure 5.5 RRC filtered π/4-QPSK signal after PA operating at P_{1dB} with p=5

5.3 Nonlinearity Effects on BER Performance for PSK-type Modulation Schemes

Nonlinearity effects on sample points of digitally modulated PSK signals are described in detail in the previous subsections and an increase in bit error rate is naturally anticipated due to the discussed slide in the sample points' original locations. This distortion quantification is simulated to yield BER. An alternative performance evaluation parameter in this sense is error vector magnitude (EVM) characterization (explained in Section 4.4.2), which appears to be more suitable for the characterization in the transmitter side. Since no phase corruption mechanism in the PA or in the channel is foreseen for the perfectly modulated signal, there will be no comprehensive difference between EVM and BER for the case in scope, where the latter evaluation parameter is much more common for the researchers in communication. But, EVM is also used for described pragmatic reasons in the comparative characterization in the oncoming sections.

In the following subsections, first, effect of primary Rapp Model ─ introduced as an SSPA characterization model in Chapter 3 ─ parameter, namely, smoothness factor p, on BER distortion is investigated. Second, effect of RRC filter roll-off factor α as a signal's parameter is discussed. Finally, BER performance results of four PSK schemes under nonlinearity are comparatively examined.

5.3.1 Effect of Smoothness Factor *p* on BER Performance

For a phase modulation scheme, Figure 5.6 gives a conceptualised BER vs. input backoff from P_{1dB} graphic (exaggerated) for two different p values at some E_b/N_o. It can be easily seen that for low and high backoffs, respectively, BER converges to same values whatever E_b/N_0 is.

For demonstrating the effect of variation of p on PSK modulation schemes, RRC filter α is fixed to 0.65 that is found to be close to the optimum value that minimizes the nonlinear distortion effects (explained in Section 4.5). The resultant graphics (Figures 5.7-5.10) are plotted as BER versus input backoff from P_{1dB}, which characterizes the operating point power, *i.e.*, related PA's P_{1dB} minus signal's average power in decibel scale. Two p values' results are illustrated in each plot, p=0.8 and p=5. Two separated plots are drawn at two different signal-to-noise ratio values: E_b/N_0=6 dB and E_b/N_o=11dB, where the new approach for the determination of BER (see Appendix B) is used for the latter case. BER results are given with 99% confidence intervals, [4].

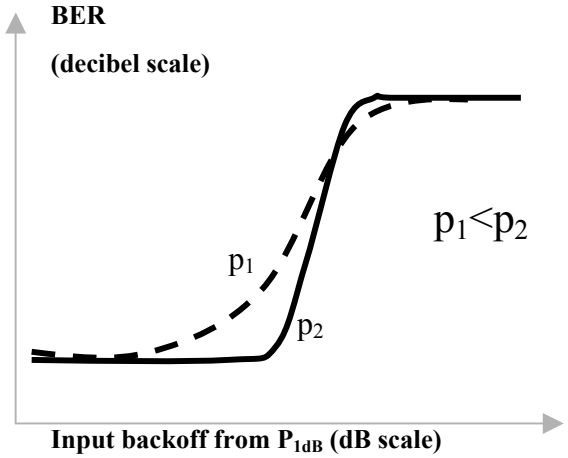

Figure 5.6 Conceptualised BER vs. input backoff from P_{1dB} plot

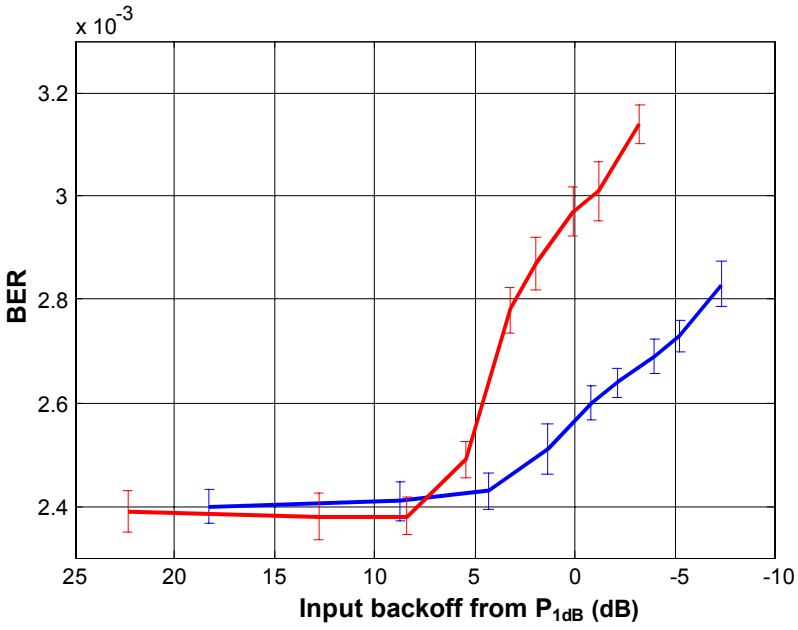

(a)

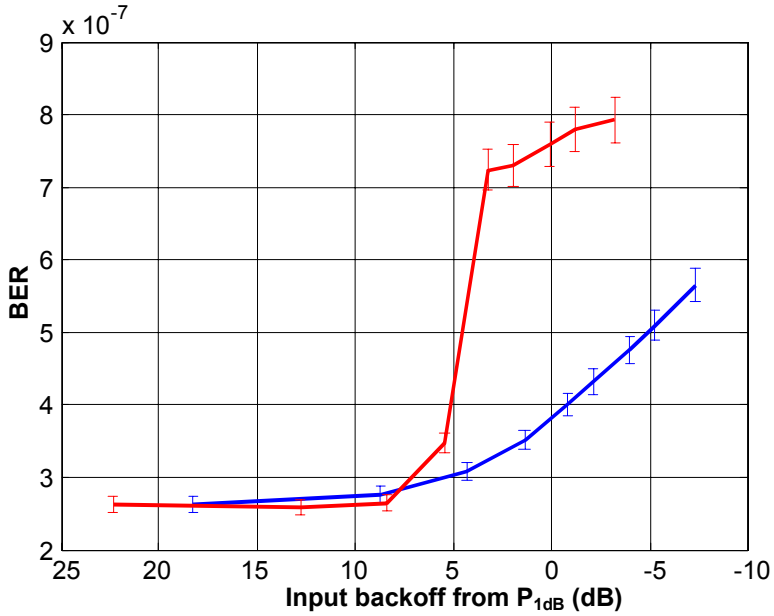

(b)

Figure 5.7 BPSK BER vs. input backoff from P_{1dB} curves (a) at E_b/N_o= 6 dB (b) at E_b/N_o= 11 dB for RRC filter α=0.65, blue: p=0.8 red: p=5

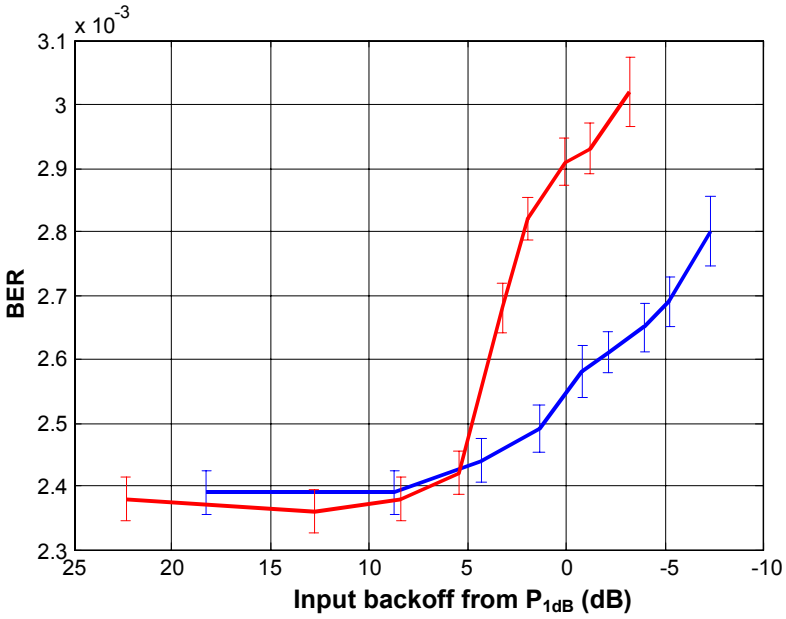

(a)

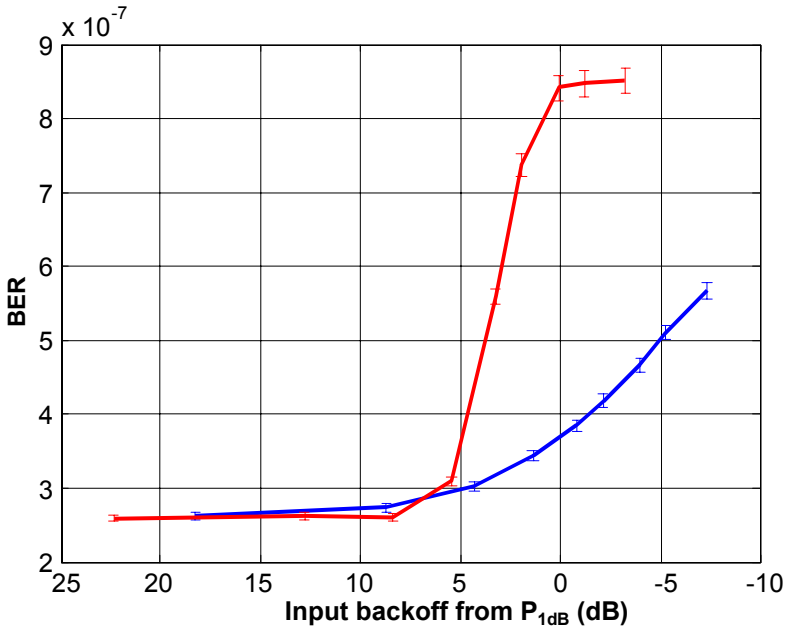

(b)

Figure 5.8 QPSK BER vs. input backoff from P_{1dB} curves (a) at E_b/N_o= 6 dB (b) at E_b/N_o= 11 dB for RRC filter α=0.65, blue: p=0.8 red: p=5

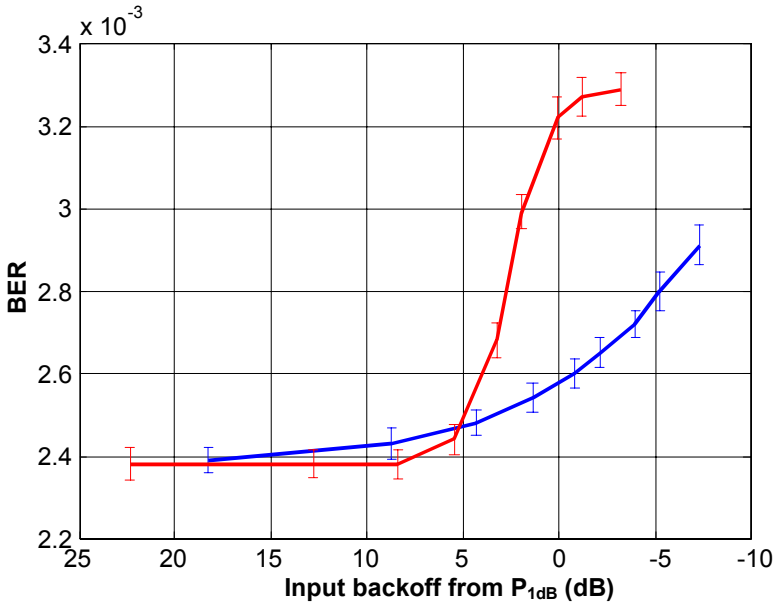

(a)

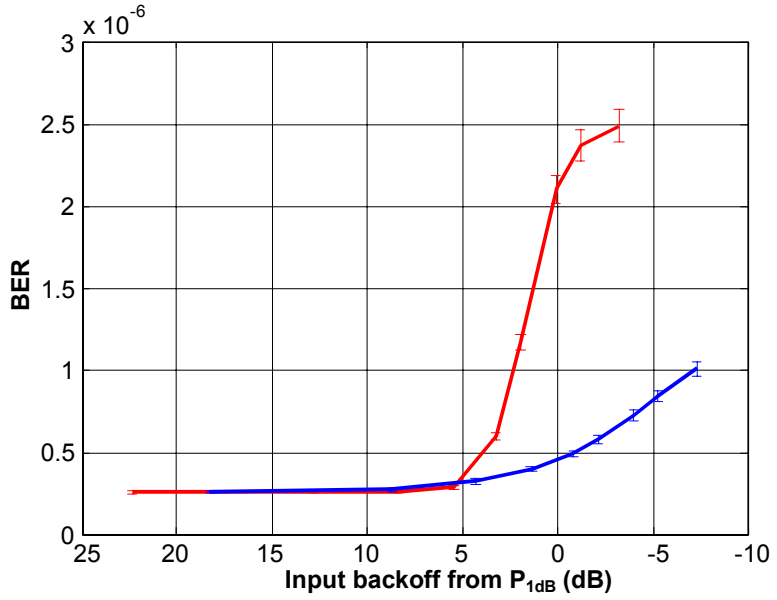

(b)

Figure 5.9 OQPSK BER vs. input backoff from P_{1dB} curves (a) at E_b/N_o= 6 dB (b) at E_b/N_o= 11 dB for RRC filter α=0.65, blue: p=0.8 red: p=5

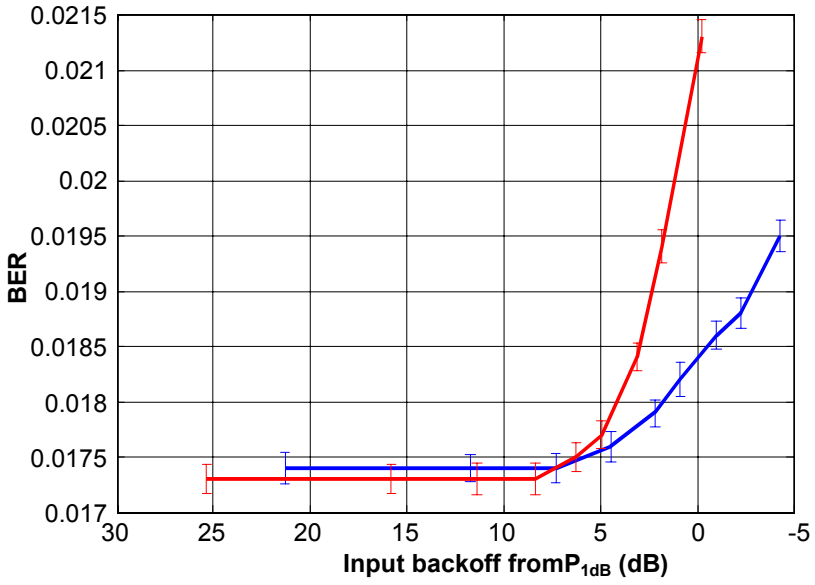

(a)

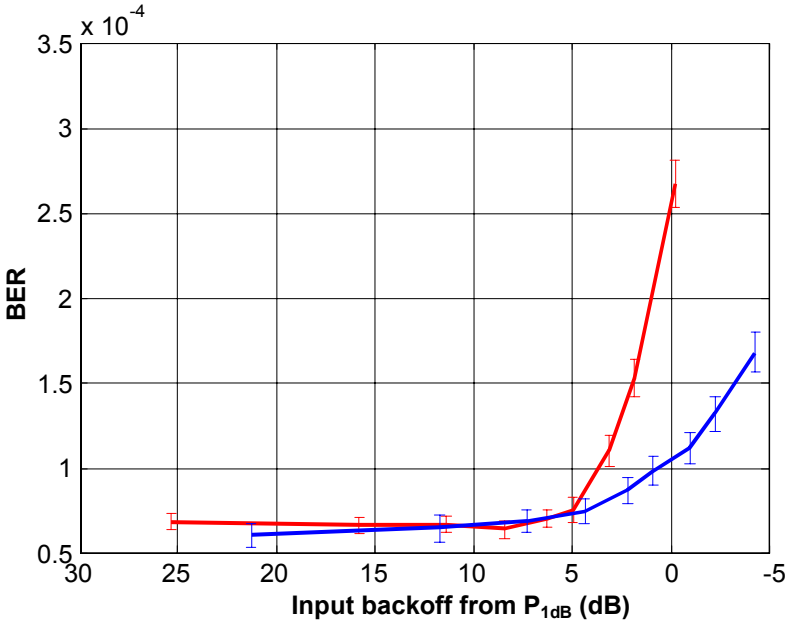

(b)

Figure 5.10 π/4-QPSK BER vs. input backoff from P_{1dB} curves (a) at E_b/N_o= 6 dB (b) at E_b/N_o= 11 dB for RRC filter α=0.65, blue: p=0.8 red: p=5

In practice, basic difference between *p* values for a phase modulation scheme is the fact that high *p* valued PA characteristic offers a wider linear range to the operational signal than small *p* valued PA characteristic at even small input P_{1dB} backoffs. At these operating points, mentioned phenomenon consequently decreases nonlinear distortion for signals at high *p* valued PA characteristic. When operating point approaches and reaches P_{1dB}, BER characteristic of signal exposed to high *p* valued characteristic deteoriorates in a rapid and significant way compared to that of small *p* valued characteristic. The main reason seems to be the much harder clipping effect on the time domain signal realized by high *p* valued PA characteristic. These statements, without any exception, are valid for all modulation schemes in scope.

5.3.2 Effect of RRC Filter Roll-off Factor on BER Performance

For demonstrating the effect of variation of α on PSK modulation schemes under nonlinearity, E_b/N_o value is fixed to 11 dB, since graphical tendency of E_b/N_o=6 dB curve will be identical to that of E_b/N_o=11 dB curve. The resultant graphics are, again, plotted as BER versus input P_{1dB} backoff value. Three α values' results are illustrated in each plot, α=0.35, α=0.65, and α=0.95, where the new approach for the determination of BER is used. BER results are given with 99% confidence intervals (see Figures 5.11-5.14).

Considering all modulation schemes, for low valued roll-off factors (*e.g.*, α=0.35), characteristics exhibit greater BER distortion under nonlinear conditions, which is solely mitigated with increasing this parameter to an extent. This α value is shown to be α=0.65 for all schemes other than OQPSK (explained in Section 4.5.1), which has a strictly decreasing BER characteristic with increasing α values.

Besides, OQPSK is the modulation scheme that is most prone to the roll-off variations, *i.e.*, varying roll-off factor of the RRC filter constitutes a more severe effect for OQPSK than others.

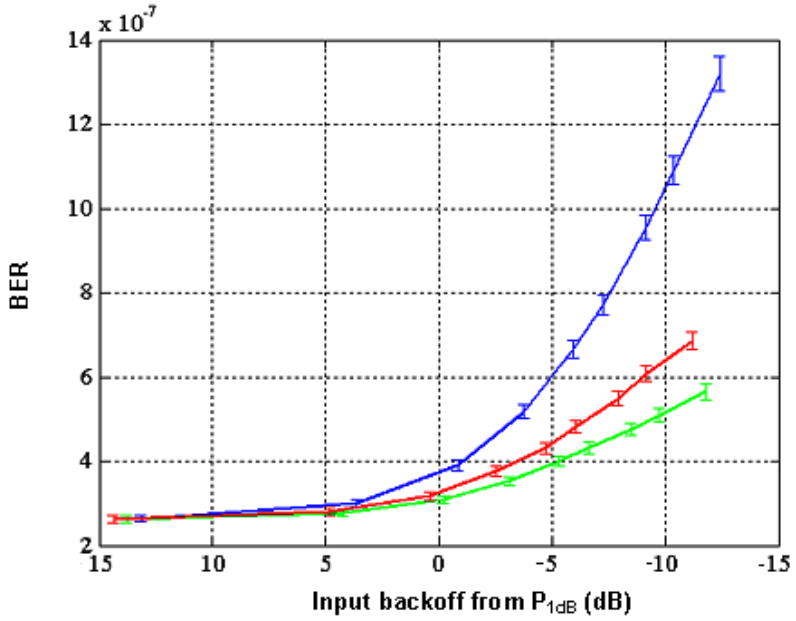

(a)

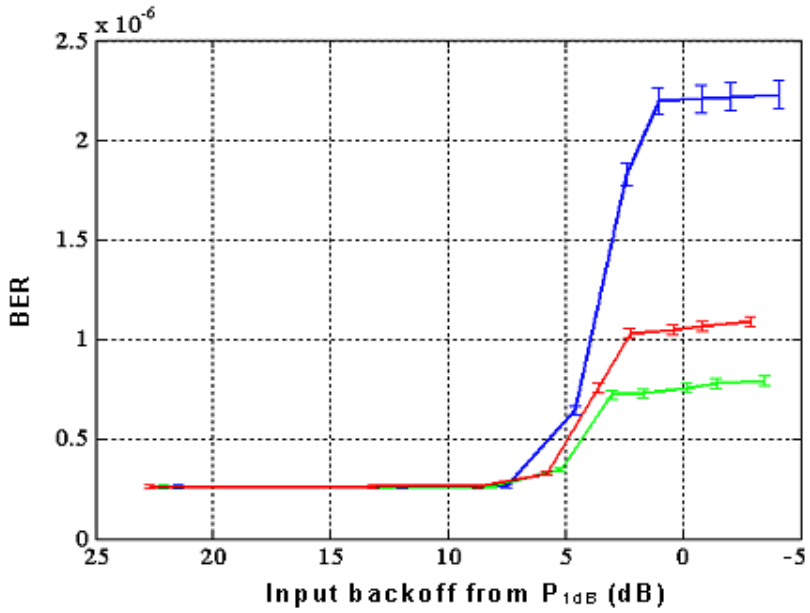

(b)

Figure 5.11 BPSK BER vs. input backoff from P_{1dB} curves at E_b/N_o=11, blue: α=0.35, green: α=0.65 red: α=0.95, (a) p=0.8 (b) p=5

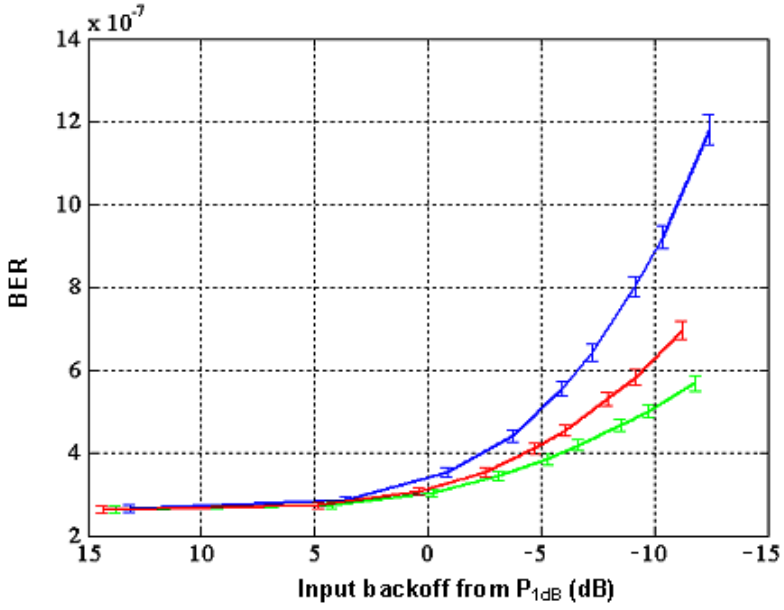

(a)

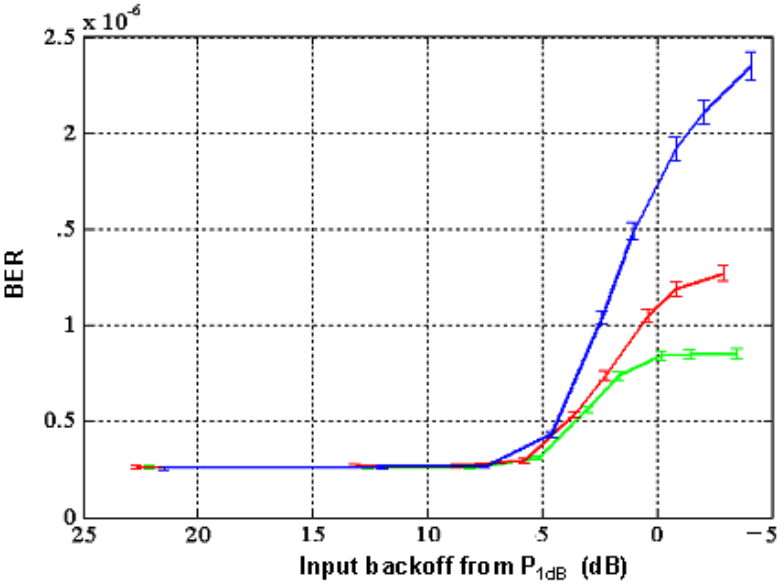

(b)

Figure 5.12 QPSK BER vs. input backoff from P_{1dB} curves at E_b/N_o=11,blue: α=0.35, green: α=0.65, red: α=0.95, (a) p=0.8 (b) p=5

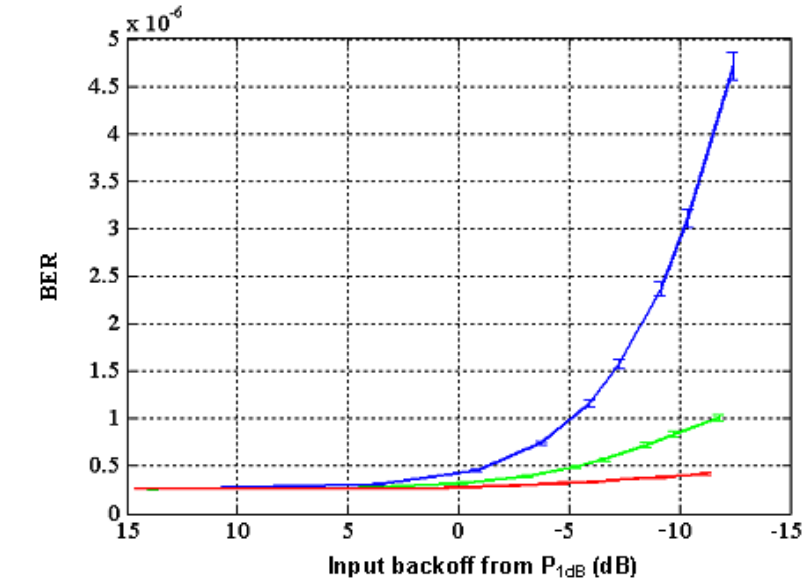

(a)

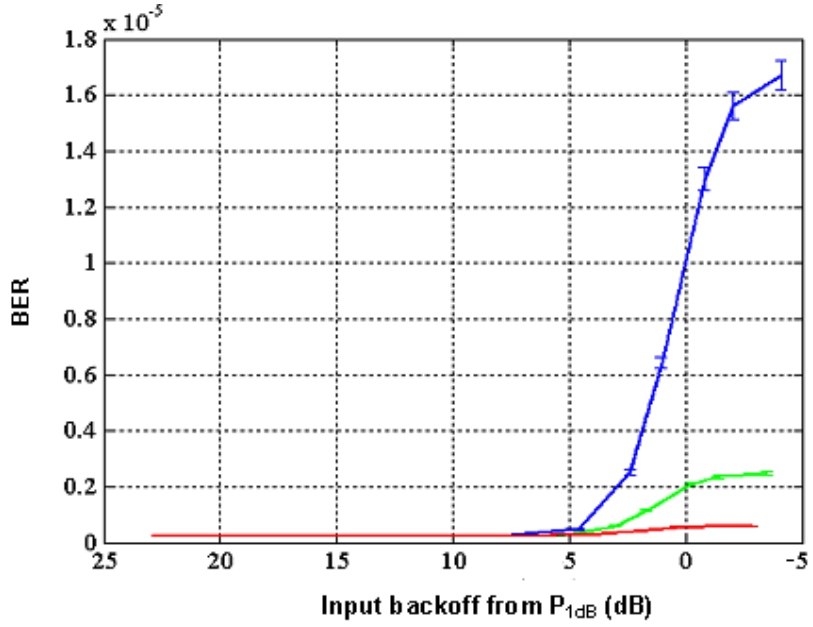

(b)

Figure 5.13 OQPSK BER vs. input backoff from P_{1dB} curves at E_b/N_o=11, blue: α=0.35, green: α=0.65, red: α=0.95, (a) p=0.8 (b) p=5

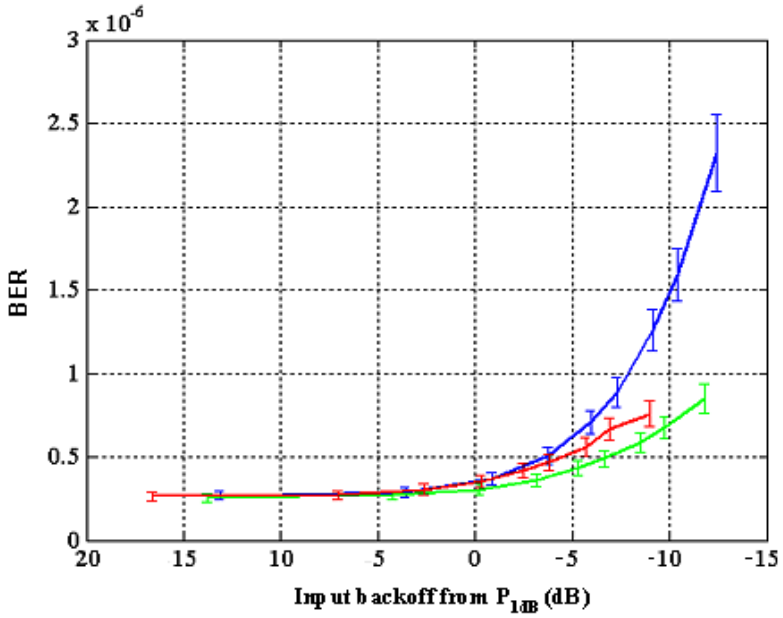

(a)

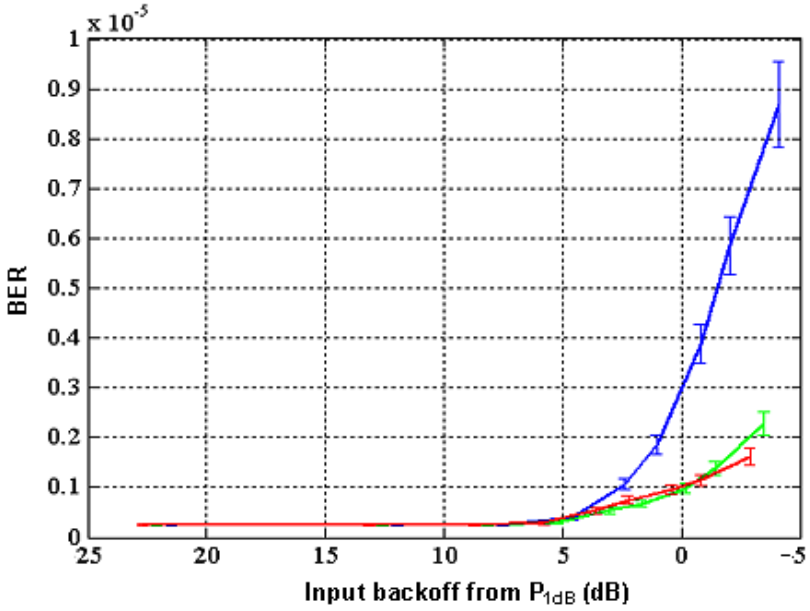

(b)

Figure 5.14 π/4-QPSK BER vs. Input P_{1dB} curves at E_b/N_o=11, blue: α=0.35, green: α=0.65, red: α=0.95, (a) p=0.8 (b) p=5

5.3.3 Comparative Performance Results Among PSK-type Modulation Schemes Under Nonlinearity

After observing effects of important PA and filter parameters, p and α, it is highly necessary to give a comparative discussion of BER performance among nonlinearly processed modulation schemes in scope. But demonstrating BER curves of all four schemes in the same graphic is difficult since BER vs. SNR characteristic of π/4-QPSK is different from those of the other three (see Section 2.5.2). So it is expressive to use another figure of merit, namely, EVM (explained in Section 4.4.2) to be able to include π/4-QPSK in demonstrations. This will also help to realize the closeness between two performance parameters (BER and EVM) in the study. So, comparison attempts are divided into two main areas.

In the first part, resultant graphics are plotted as BER versus input backoff value for BPSK, QPSK, and OQPSK. In these plots, signal-to-noise ratio values are 6 and 11 dB, α values are 0.35 and 0.95, and p values are 0.8 and 5. BER results are given with 99% confidence intervals. The results of the first part are shown in Figures 5.15-5.22.

These examples demonstrate that, for low roll-off values, BPSK and QPSK are more resistant to specific SSPA nonlinear distortion compared to OQPSK, whereas for high roll-off values, OQPSK performs much better.

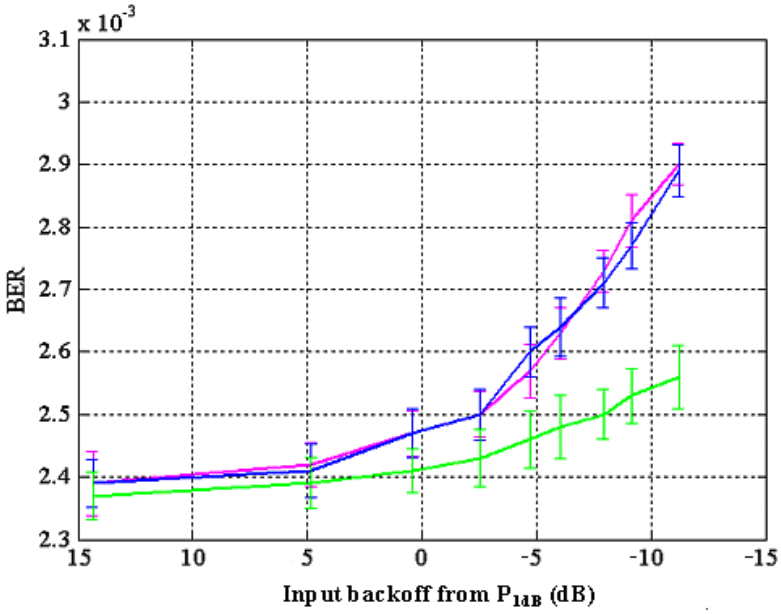

Figure 5.15 BER vs. input backoff from P_{1dB} curves at E_b/N_o= 6 dB, α=0.95, p=0.8, blue:QPSK magenta: BPSK, green: OQPSK

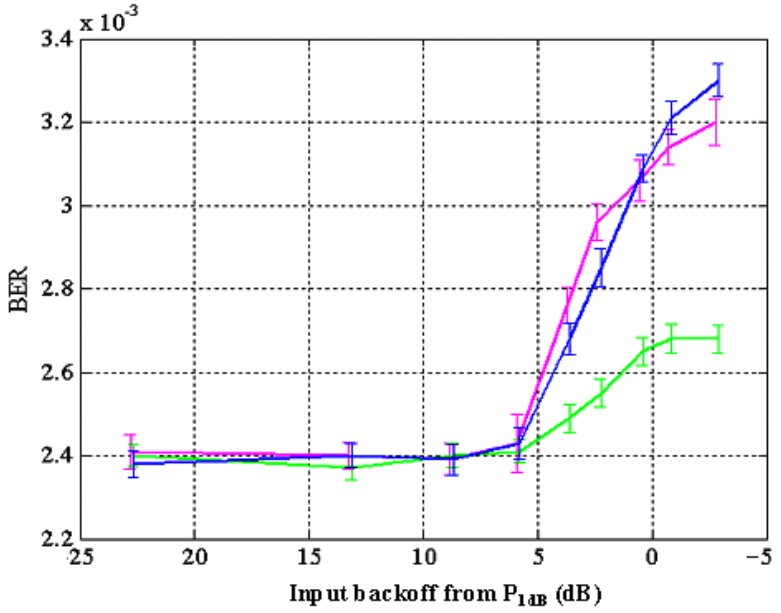

Figure 5.16 BER vs. input backoff from P_{1dB} curves at E_b/N_o= 6 dB, α=0.95, p=5, blue:QPSK, magenta: BPSK, green: OQPSK

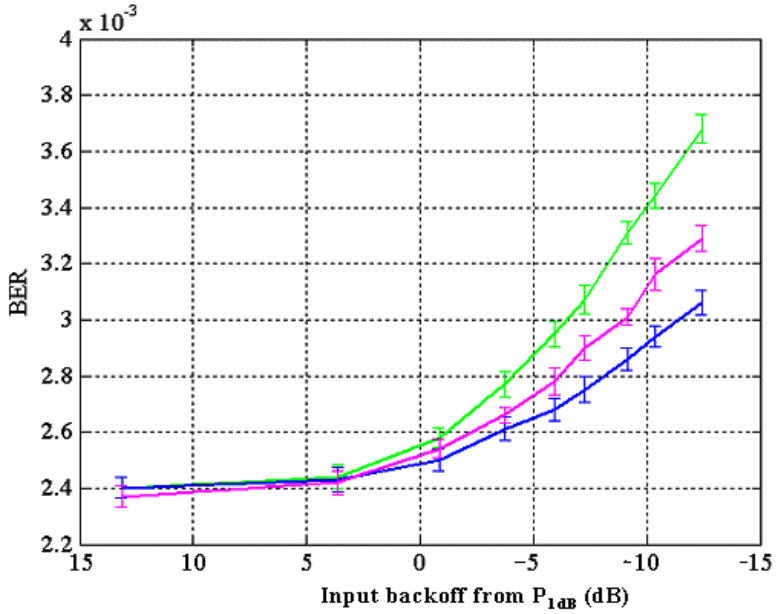

Figure 5.17 BER vs. input backoff from P_{1dB} curves at E_b/N_o= 6 dB, α=0.35, p=0.8, blue:QPSK, magenta: BPSK, green: OQPSK

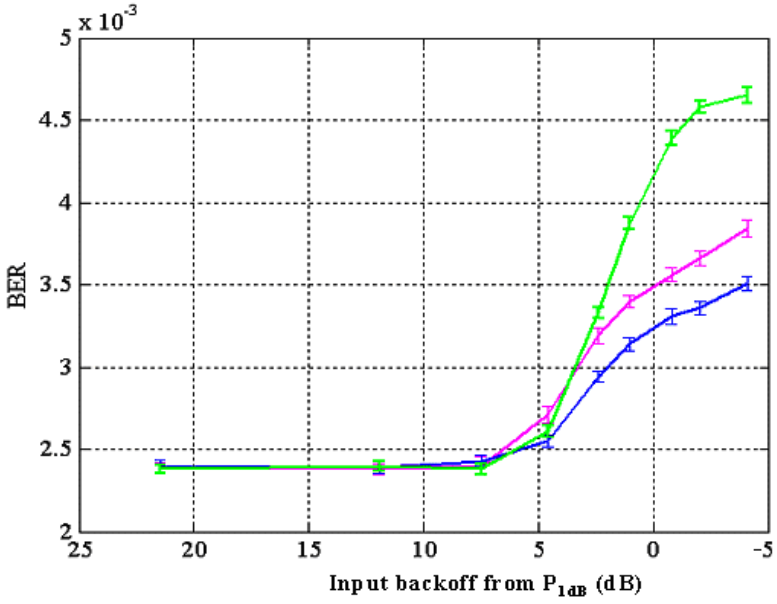

Figure 5.18 BER vs. input backoff from P_{1dB} curves at E_b/N_o= 6 dB, α=0.35, p=5, blue:QPSK, magenta: BPSK, green: OQPSK

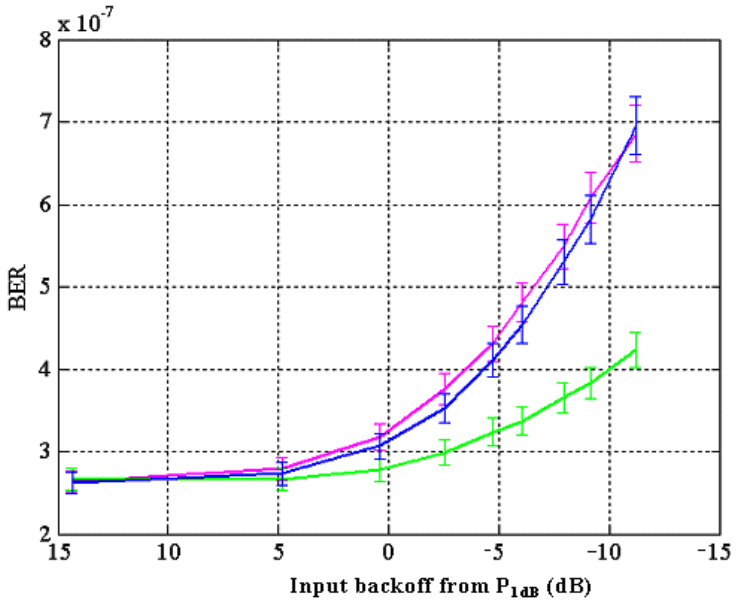

Figure 5.19 BER vs. input backoff from P_{1dB} curves at E_b/N_o= 11 dB, α=0.95, p=0.8, blue:QPSK magenta: BPSK, green: OQPSK

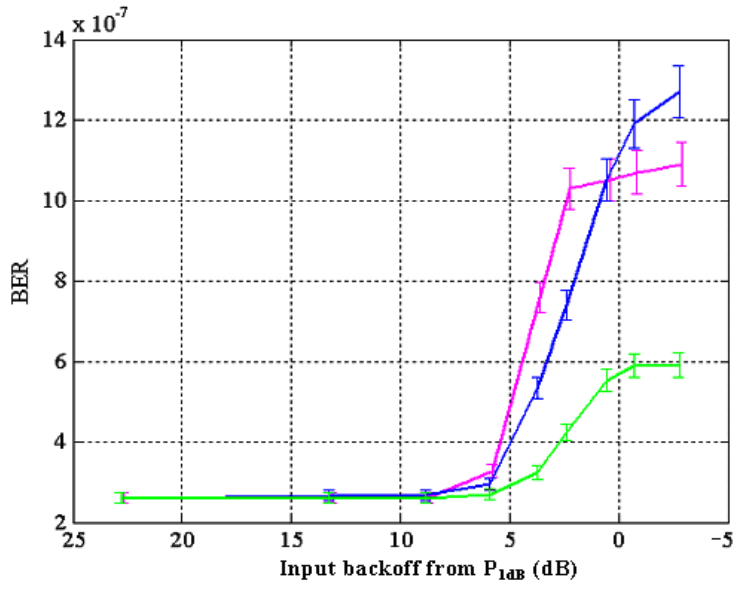

Figure 5.20 BER vs. Input P_{1dB} curves at E_b/N_o= 11 dB, α=0.95, p=5, blue:QPSK magenta: BPSK, green: OQPSK

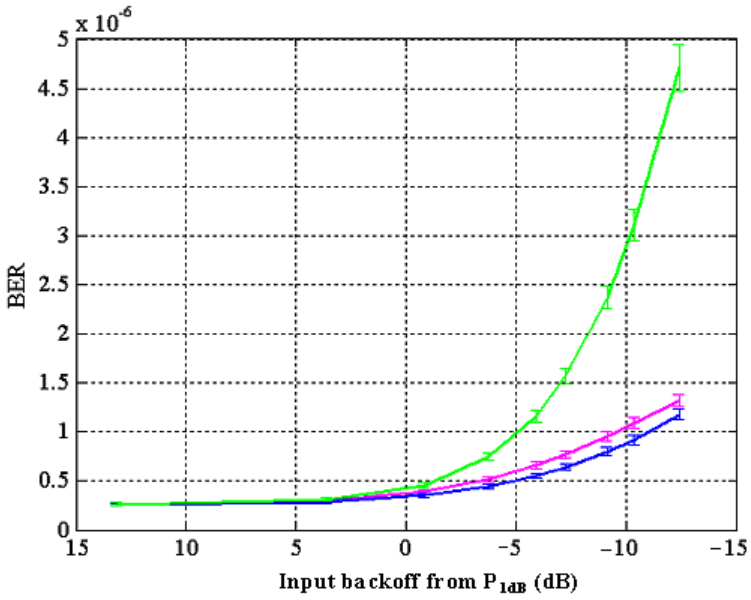

Figure 5.21 BER vs. input backoff from P_{1dB} curves at E_b/N_o= 11 dB, α=0.35, p=0.8, blue:QPSK magenta: BPSK, green: OQPSK

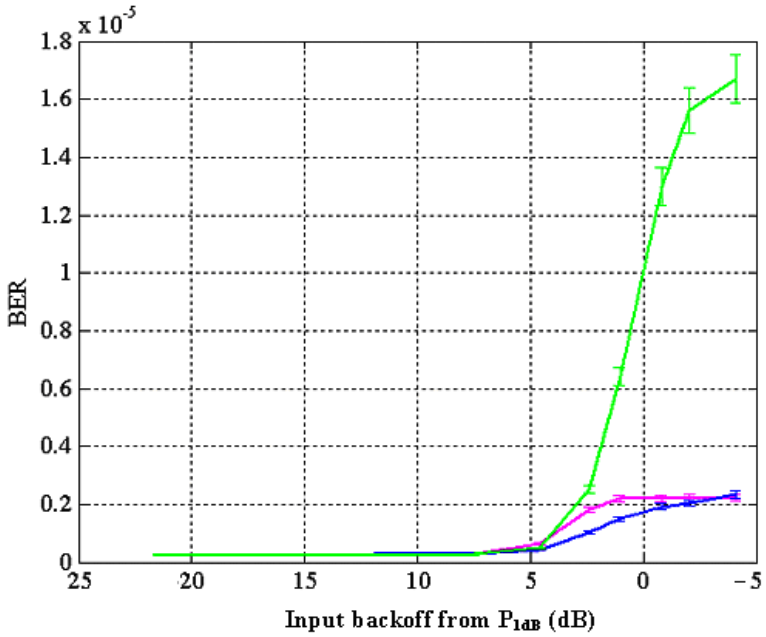

Figure 5.22 BER vs. Input P_{1dB} curves at E_b/N_o= 11 dB, α=0.35, p=5, blue:QPSK magenta: BPSK, green=OQPSK

As filter roll-off factor decreases, filter bandwidth also decreases and transient fluctuations during phase transitions become stronger and increase BER. Since OQPSK samples are twice as much compared to other PSK schemes, OQPSK is affected more adversely as the roll-off factor decreases. This effect becomes more pronounced for higher values of p.

CCDF observation (see Figures 4.9-4.11) also supports this time domain clarification. For the same modulation parameters (including average power) OQPSK's power deviation from the average is obviously the smallest for high roll-off.

For low roll-off values, OQPSK's power deviation from the average is not significantly different from the other schemes while its BER performance is the worst. The reason can be the fact that, in OQPSK, quadrature data samples are conveyed individually in the signal with half-period apart in an offset manner, not together on the same point as in the other three PSK schemes. This modulation mentality difference between schemes may mean less tolerance against nonlinear distortion for low roll-off values.

In the second part, resultant graphics are plotted as EVM_{rms} versus input backoff value for three quadrature PSK schemes, namely, QPSK, OQPSK, and π/4-QPSK. In these plots, E_b/N_o value is taken as infinity, to simply isolate the effect of PA's nonlinearity. Besides, α values are 0.35 and 0.95 and p values are 0.8 and 5. EVM_{rms} versus input backoff results are shown in Figures 5.23-5.26, which are additionally given for two main facts. First one is to strengthen the comments – made as the results of BER discussions – by giving related graphics. Second one is to be able to demonstrate comparative nonlinear distortion effects including π/4-QPSK modulation which does not lend itself to comparison in BER evaluation. This stems from the fact that theoretical BER vs. SNR curves of BPSK, QPSK, and OQPSK are exactly the same, whereas that of π/4-QPSK is different.

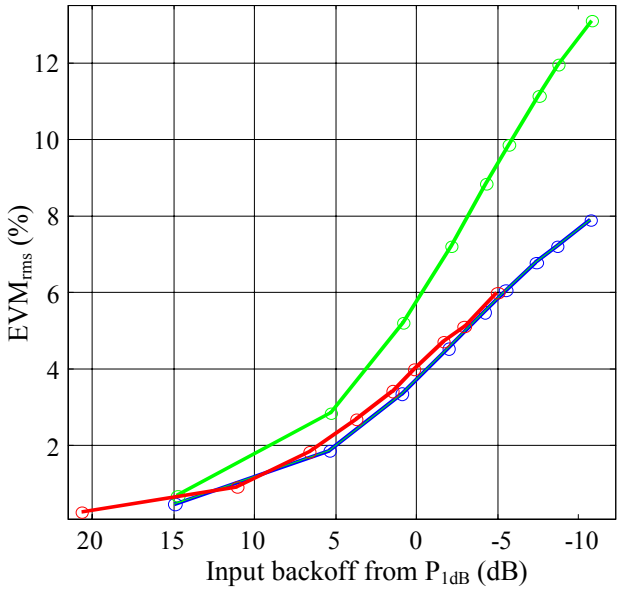

Figure 5.23 EVM$_{rms}$ vs. input backoff results for p=0.8, α=0.35, blue: QPSK, red: π/4-QPSK, green: OQPSK

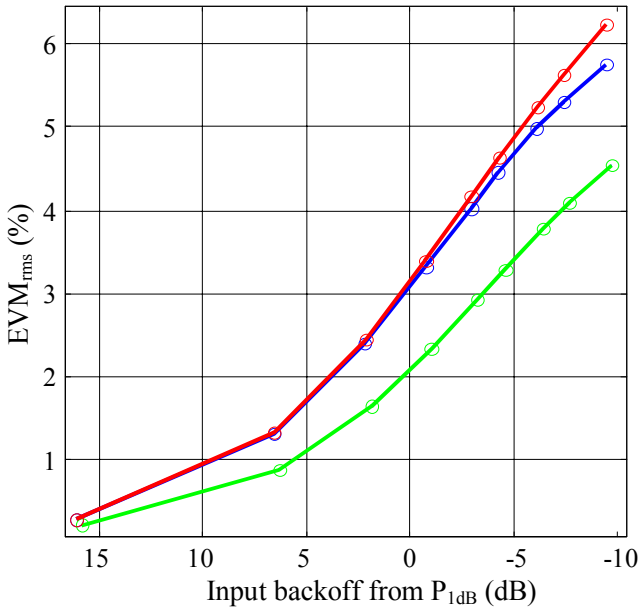

Figure 5.24 EVM$_{rms}$ vs. input backoff results for p=0.8, α=0.95, blue: QPSK, red: π/4-QPSK, green: OQPSK

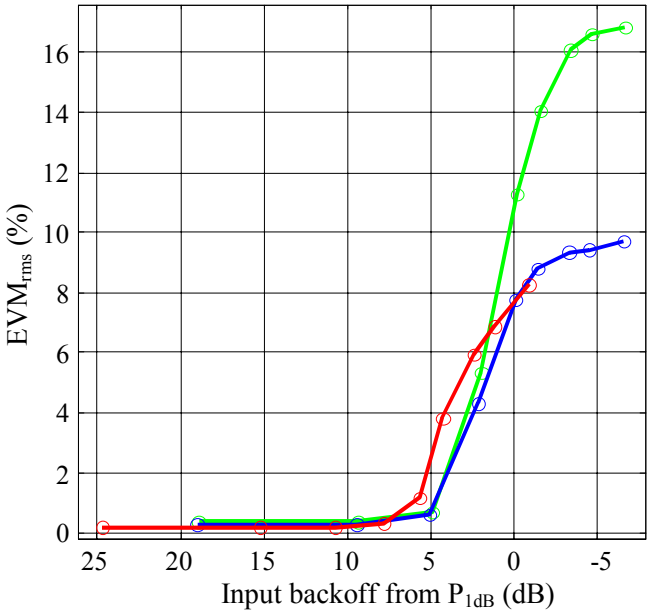

Figure 5.25 EVM_{rms} vs. input backoff results for p=5, α=0.35, blue: QPSK red: π/4-QPSK, green: OQPSK

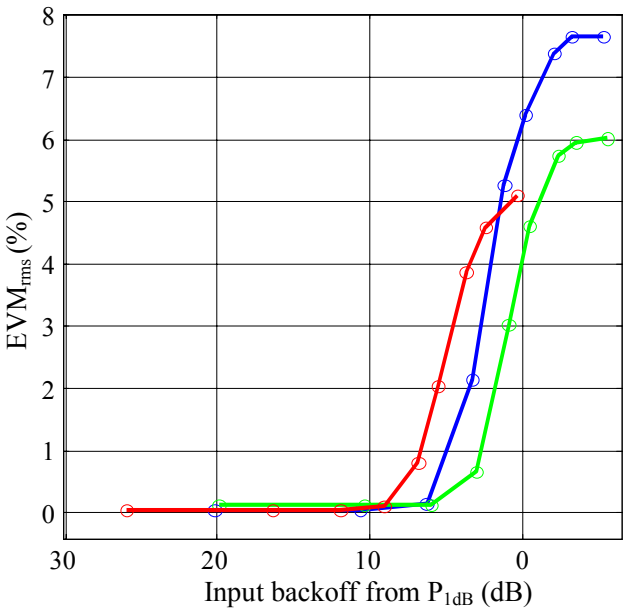

Figure 5.26 EVM_{rms} vs. input backoff results for p=5, α=0.95, blue: QPSK red: π/4-QPSK, green: OQPSK

As seen, especially for PA characteristic with low p values (*e.g.*, p=0.8), the distortion characteristic of π/4-QPSK modulation is almost the same as that of QPSK. When compared to these two schemes, OQPSK's behaviour is just as explained in Section 5.3.2 where there is a significant variation in the curves with RRC filter α, especially for PA operating at high p values (*e.g.*, p=5).

5.4 Nonlinearity Effects in Comparison with SFCG 21-2 Spectral Mask

Effects of memoryless nonlinear processes on a digital-modulated signal's spectral characteristics are theoretically described in Section 4.4.3.1. In the following subsections, results of the simulations for each selected PSK-modulated signals (BPSK, QPSK, OQPSK, π/4-QPSK), exposed to nonlinear PA operation are given. The Welch spectral estimation method (see Appendix C) is used to obtain spectral characteristics after PA, where resulting spectra are assessed in comparison with SFCG 21-2 spectral mask. In this respect, backoff value is given when the corresponding spectrum reaches this mask. p value corresponding to PA characteristic and signal's RRC filter α value are performance comparison parameters for a modulation scheme. Finally, schemes' evaluation is also given.

5.4.1 QPSK

Normalized PSD of a QPSK modulated signal, having three different RRC filter α values, is plotted against frequency normalized to the symbol rate – being the convention used by SFCG in [22] – in the following QPSK plots. First of all, Figure 5.27 shows PA operating in the linear region and is given for comparison.

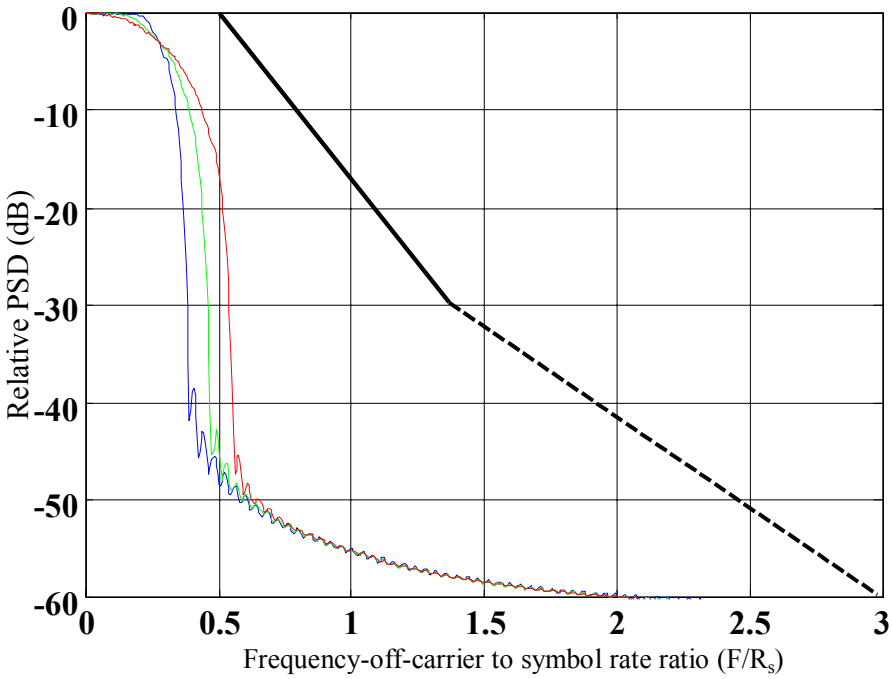

Figure 5.27 SFCG 21-2 Spectral Mask and QPSK modulated signal spectra for a PA operating in the linear region, blue: α= 0.35, green: α= 0.65, red: α= 0.95

It is obvious that there is no stress for signals in satisfying the spectral mask constraint in this situation.

The following figures demonstrate the same signals' spectra when they experience PA nonlinearity. Table 5.1 demonstrates the numerical values of limiting backoffs for each case.

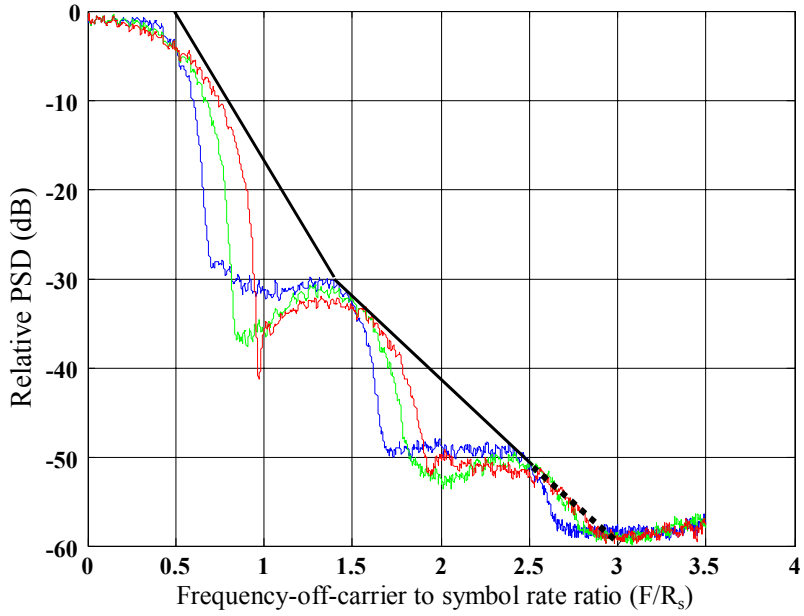

Figure 5.28 Signal spectra when PA (p=0.8) operates at limiting backoffs, blue: α=0.35, green: α=0.65, red: α=0.95, for QPSK

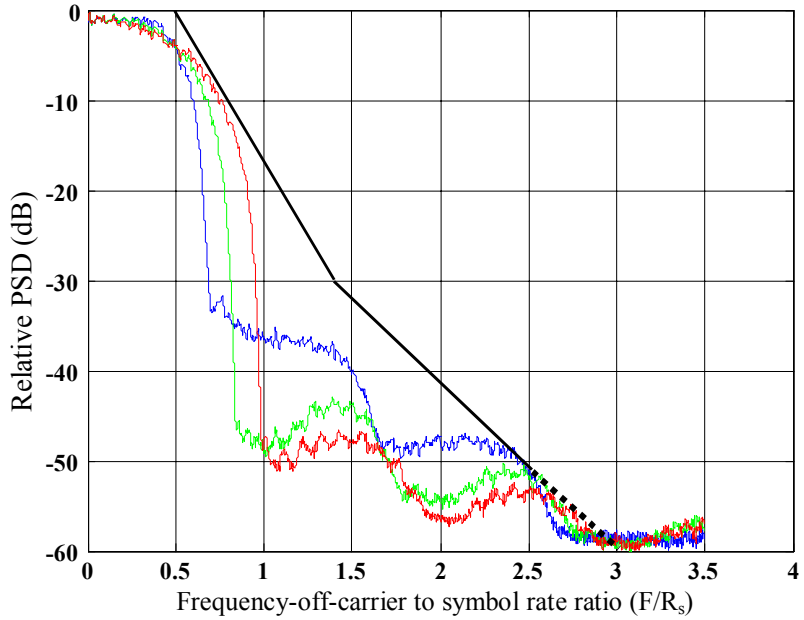

Figure 5.29 Signal spectra when PA (p=5) operates at limiting backoffs, blue: α=0.35, green: α=0.65, red: α=0.95, for QPSK

Table 5.1 Limiting backoff values in Figures 5.28-5.29

p / RRC filter *α*	**0.8**	**5**
0.35	-1.47	5.60
0.65	0.96	6.97
0.95	2.74	7.71

As can be inferred from above figures, QPSK spectrum shows a stair-like characteristic under nonlinearity, which is an example of spectral regrowth phenomenon (see Section 4.4.3.1). Besides, for both PA's *p* characteristics, with increasing RRC filter α values, signal spectra arrive the mask for lower backoff values.

Again, it can be concluded that, for the same RRC filter α, lower *p* valued characteristics permit lower PA backoff values. The last inference can be the relative sidelobe levels occurring under nonlinearity for different *p* values. For low values of this parameter, each sidelobe amplitude gets higher in a balanced way under nonlinearity. For a high value of *p*, the second sidelobe grows more rapidly than the first one, causing spectral mask violation.

Thus, choosing both lower RRC filter α value and lower *p* valued PA offers better usage of spectrum at a higher limiting PA backoff value ─ permitting higher power output ─ for QPSK modulation.

5.4.2 OQPSK

Normalized PSD of an OQPSK modulated signal is the same as that of QPSK given in Figure 5.27. For a linear amplifier, Figures 5.30-5.31 demonstrate OQPSK signals' spectra with three different RRC filter α values when they experience PA nonlinearity. Table 5.2 shows the corresponding limiting backoff values.

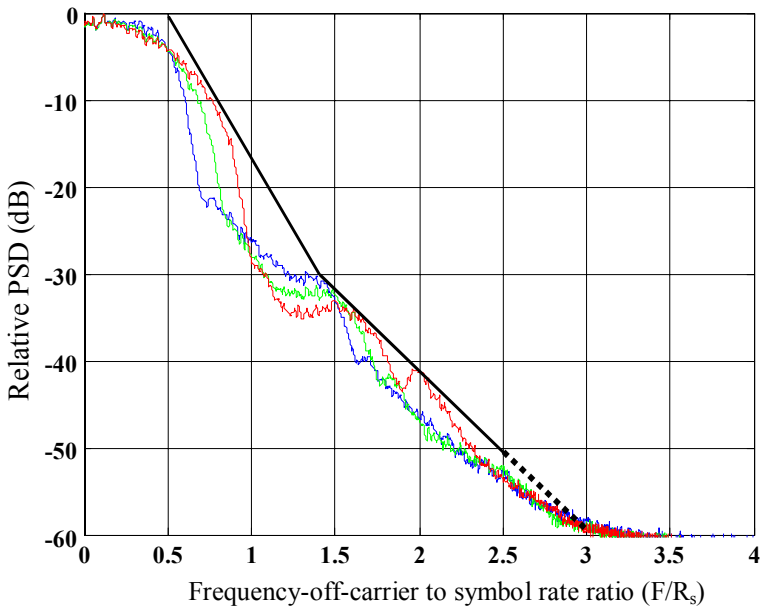

Figure 5.30 Signal spectra when PA (p=0.8) operates at limiting backoffs, blue: α=0.35, green: α=0.65, red: α=0.95, for OQPSK

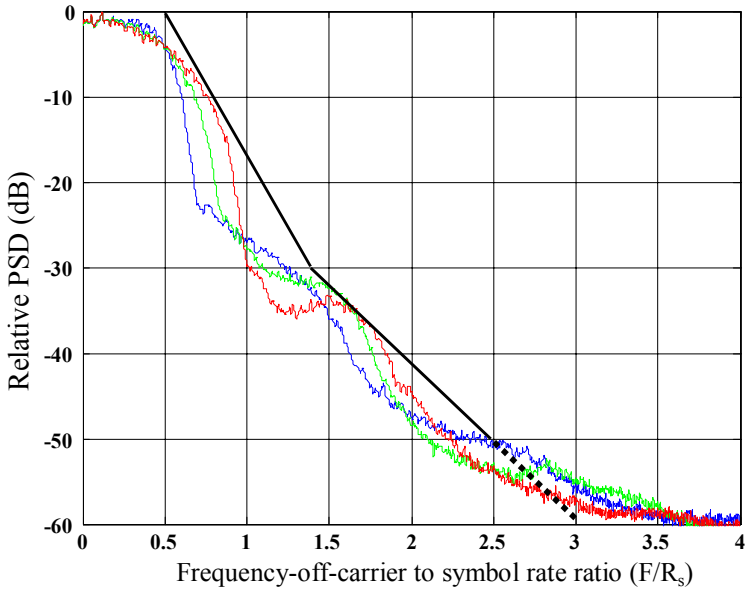

Figure 5.31 Signal spectra when PA (p=5) operates at limiting backoffs, blue: α=0.35, green: α=0.65, red: α=0.95, for OQPSK

Table 5.2 Limiting backoff values in Figures 5.30-5.31

RRC filter α \ p	**0.8**	**5**
0.35	-6.64	3.73
0.65	-6.30	3.40
0.95	-5.70	3.67

OQPSK modulation primarily lessens the fluction in the envelope of the QPSK signal, which can be seen from CCDF discussions (see Section 4.6). This arises as a consequence of the modulation mentality difference between these two quadrature modulation types.

For OQPSK modulated signal under nonlinearity, this difference also seems to smooth out the spectral transition characteristic of nonlinearly amplified QPSK described above and makes OQPSK more fit to the SFCG 21-1 spectral mask. A

comparison of these two PSK modulation schemes shows that lower limiting backoff values are achieved for OQPSK than those of QPSK for all cases.

The effects of RRC α and PA *p* values under nonlinear process tend to be similar with that of QPSK characteristics.

5.4.3 Π/4-QPSK

Normalized PSD of a π/4-QPSK modulated signal is the same as that of QPSK given in Figure 5.27. For a linear amplifier, Figures 5.32-5.33 demonstrate π/4-QPSK signals' spectra with three different RRC filter α values when they experience PA nonlinearity. Table 5.3 shows the corresponding limiting backoff values.

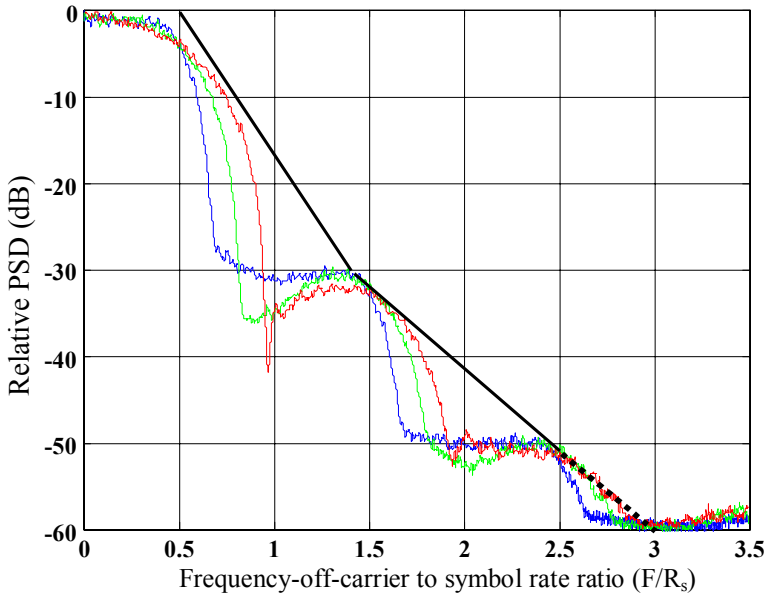

Figure 5.32 Signal spectra when PA (*p*=0.8) operates at limiting backoffs, blue: α=0.35, green: α=0.65, red: α=0.95, for π/4-QPSK

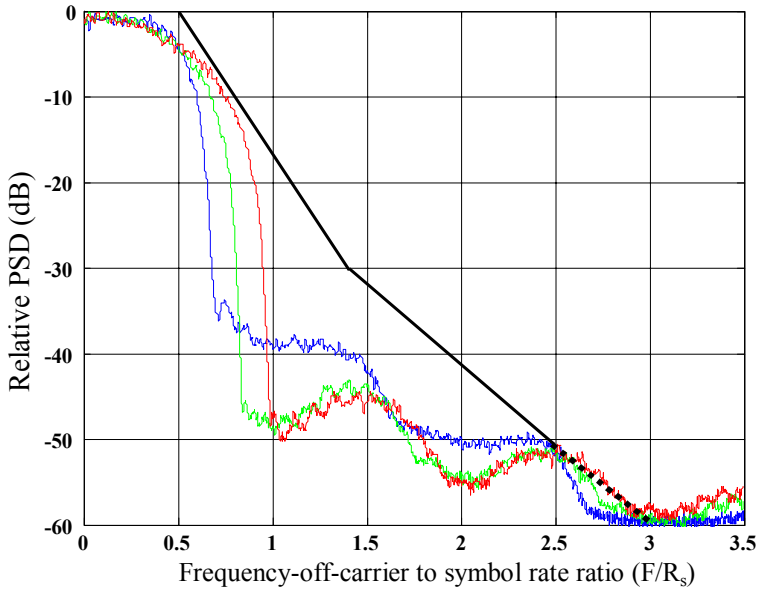

Figure 5.33 Signal spectra when PA (p=5) operates at limiting backoffs, blue: α=0.35, green: α=0.65, red: α=0.95, for π/4-QPSK

Table 5.3 Limiting backoff values in Figures 5.32-5.33

RRC filter α \ p	**0.8**	**5**
0.35	-1.49	5.89
0.65	0.67	6.95
0.95	2.57	7.40

For the considered nonlinearities, π/4-QPSK can be said to be no different from QPSK in spectral sense. This can also be inferred from CCDF curve similarities between these two schemes. Also, the effects of RRC α and PA p values under nonlinear process tend to be similar to that of QPSK characteristics.

5.4.4 BPSK

Normalized PSD of a BPSK modulated signal is the same as that of QPSK given in Figure 5.27. For a linear amplifier, Figures 5.34-5.35 demonstrate signals' spectra with three different RRC filter α values when they experience PA nonlinearity. Table 5.4 shows the corresponding limiting backoff values.

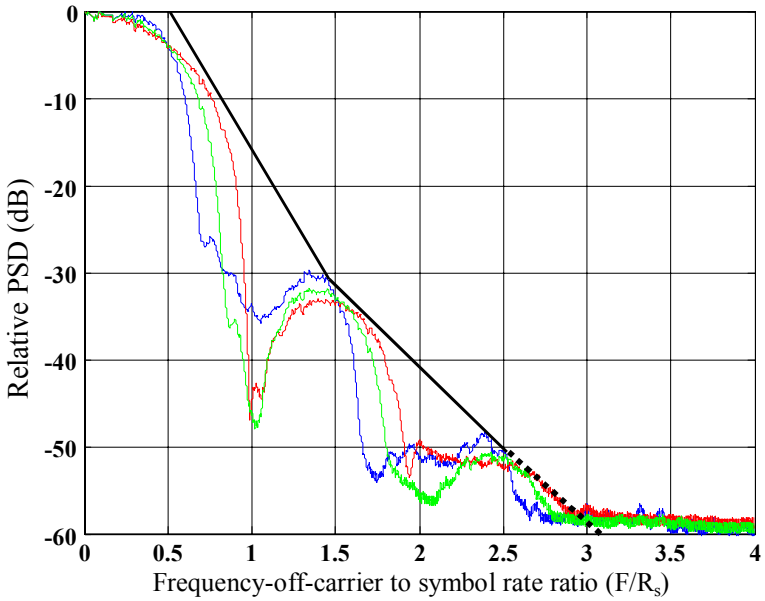

Figure 5.34 Signal spectra when PA (p=0.8) operates at limiting backoffs, blue: α=0.35, green: α=0.65, red: α=0.95, for BPSK

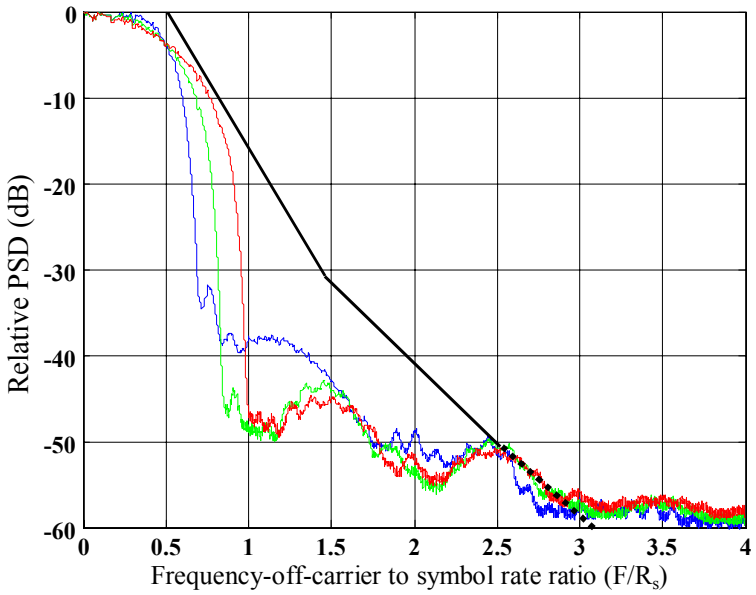

Figure 5.35 Signal spectra when PA (p=5) operates at limiting backoffs, blue: α=0.35, green: α=0.65, red: α=0.95, for BPSK

Table 5.4 Limiting backoff values in Figures 5.34-5.35

RRC filter α \ p	**0.8**	**5**
0.35	-1.27	6.81
0.65	3.24	7.44
0.95	4.42	7.86

For the considered nonlinearities, BPSK seems to be a little worse than QPSK in spectral sense. But, the effects of RRC α and PA p values under nonlinear process tend to be similar to that of QPSK characteristics. It must be remembered that BPSK can only handle half bit rate relative to other three quadrature modulation schemes for the same bandwidth.

CHAPTER 6

CONCLUSIONS AND FUTURE WORK

The study presented in this work deals with the basic effects of nonlinearity on the performance of selected four phase shift keying (PSK) type modulation schemes ─ BPSK, QPSK, OQPSK, and π/4-QPSK ─ in the special case of a solid state power amplifier (SSPA) nonlinearity. This is achieved by selecting an appropriate power amplifier (PA) nonlinearity model commonly accepted in the related literature and by investigating the effects of different nonlinearities of a PA by varying a specific parameter of this model. The performance is evaluated by simulations on MATLAB®. For the modulation performance evaluation, a variety of criteria are used. Namely, for the assessment of the quality of communication

- Bit error ratio (BER)
- Error vector magnitude (EVM)

are utilized and for the assessment of the spectral performance

- Space Frequency Coordination Group (SFCG) spectral mask

is utilized. In the determination of parameters to be used in simulations, the modeling of a specific high power amplifier (HPA), designed at TÜBİTAK-BİLTEN, was the primary motivation.

As a result of this study, following conclusions can be drawn:

- Modulation schemes show different BER performances against selected nonlinearity model (Rapp model) with different root raised cosine (RRC) transmit-receive filter rolloff factors α. BPSK and QPSK, each, have an optimum α in this sense, where BER performances of OQPSK and π/4-QPSK monotonically get better with increasing α. Complementary cumulative distribution function (CCDF) of OQPSK modulation shows a clear distinction compared to those of BPSK, QPSK, π/4-QPSK whose corresponding curves are close to eachother. Hence, for all α values, roughly, the ratio of peak power level to average power level of OQPSK is significantly smaller than those of other three. It must also be noted that various nonlinear amplitude distortions (e.g., BER) do not have a monotonous relationship with the peak-to-average ratios of signals, [28].

- Transmitted constellation diagrams of two quadrature modulation schemes (QPSK and π/4-QPSK) show inherently different scattering characteristics under nonlinearity than that of OQPSK modulation.

- In general, a higher value of *p* parameter (abruptly changing PA characteristic) results in more distortion in the signal than a smaller value of the *p* parameter (smooth nonlinearity) under same operating conditions (backoff levels). For PA's operations closer to the P_{1dB}, the distortions become more severe.

- For lower values of α, characteristics exhibit greater BER distortion under nonlinear conditions. Thus, BER distortion can be decreased with increasing α, but only to a point for all schemes other than OQPSK which has a strictly decreasing BER characteristic with increasing α values. OQPSK is also the modulation scheme that is most prone to the roll-off variations, i.e., varying roll-off factor of the RRC filter results in a more severe change.

- For lower α values, BPSK and QPSK are more resistant to specific SSPA nonlinear distortion compared to OQPSK, whereas for high roll-off values, OQPSK performs much better. EVM results show a strict compliance with BER results as anticipated.

- For all schemes, signal spectra show spectral regrowth phenomenon when PA nonlinearity is present. All filtered signal spectra show a stair-like characteristic other than OQPSK, whose spectrum characteristic decreases gently with a fixed slope over the frequency axis, obviously suitable for mask constraint. With increasing RRC filter α values, signal spectra arrive the SFCG spectral mask for lower (numerically) backoff values for all modulation schemes. Also, lower *p* valued characteristics permit lower PA backoff values. Thus, choosing both lower RRC filter α value and lower *p* valued PA offers better usage of spectrum at a lower limiting PA backoff value ─ permitting higher power output ─ for all modulation schemes.

Finally useful conclusions can be drawn for the specific (satellite) application in scope. Since bandwidth efficiency of BPSK is half of the those of other three and theoretic BER values of π/4-QPSK are far worse than the those of QPSK/OQPSK, former two modulation schemes wouldn't be preferred. Moreover, the recommended spectral mask constraint is thought to have the second priority against the high quality communication requirement for the space applications, OQPSK modulation scheme ─ filtered with RRC filter having high α ─ turns out to be the best choice possible. Having the constant envelope property, filtered CPM also seems to be another robust modulation format against nonlinearity, but is not included in the investigations for the communication transmitter in scope does utilize only PSK schemes.

Besides these basic achievements, there are also some issues that need further study. Different nonlinearity types (i.e., with memory) and error correction coding schemes, [2], for the transmitted signal should be studied. Also, different distortion compensation structures (e.g., predistortion, [11]) utilized in the transmitter/receiver systems may be investigated.

REFERENCES

[1] Shannon C.E., "A mathematical theory of communication", *Bell System Technical Journal,* vol. 27, pp. 379-423 and 623-656, July and October, 1948.

[2] Proakis J.G., *Digital Communications*, *3rd Ed.*, McGRAW-HILL Publications, Singapore, 1995.

[3] Clarke K.K., Hess D.T., *Communication Circuits: Analysis and Design*, Addison-Wesley Publishing Company, New York, 1971

[4] Jeruchim M.C., Balaban P., K.S. Shanmugan, *Simulation of Communication Systems, 2nd Ed.,* Kluwer Academic/Plenum Publishers, New York, 2000.

[5] Saleh A.A.M., "Frequency-Independent and Frequency-Dependent Nonlinear Models of TWT Amplifiers", *IEEE Transactions on Communications,* Vol.Com-29, No.11.,pp. 1715-1720, November 1981.

[6] Fazel K., Kaiser S., "Analysis of Non-Linear Distortions on MC-CDMA", *IEEE International Conference on Communications* (ICC '98),Vol. 2, pp. 1028 - 1034, June 1998.

[7] Sevic J.F., Staudinger J., "Simulation of Power Amplifier Adjacent-Channel Power Ratio for Digital Wireless Communication Systems", *47th IEEE Vehicular Technology Conference*, Volume: 2 , 4-7 May 1997.

[8] Zhou G.T., "Analysis of Spectral Regrowth of Weakly Nonlinear Power Amplifiers", *IEEE Communication Letters,* Vol. 4, No:11, pp. 357-359, November 2000.

[9] Braithwaite R.N., "Nonlinear Amplification of CDMA Waveforms: An Analysis of Power Amplifier Gain Errors and Spectral Regrowth", *48th IEEE Vehicular Technology Conference* (VTC'98), Volume:3, 18-21 May 1998.

[10] Razavi B., *RF Microelectronics*, Prentice Hall Publications, 1998

[11] Sklar B., *Digital Communications, 2nd Ed.*, PRENTICE HALL Publications, New Jersey, 2001.

[12] Haykin S., *Communication Systems, 4th Ed.,* JOHN WILEY & SONS Publications, USA, 2001.

[13] Simon M.K., *Carrier Synchronization of Offset Quadrature Phase Shift Keying,* NASA TMO Progress report, pp. 42 –133, 1998.

[14] Evans B., *Satellite Communications B – Digital modulation,* Lecture notes, University of Surrey, pp. 49-52, Spring 2002.

[15] Liu C., Feher K., "Noncoherent detection of π/4-QPSK systems in a CCI-AWGN combined interference environment", *Proc. of IEEE Vehicular Technology Conference,* San Francisco, CA, pp. 83-94, May 1989.

[16] Miller L.E., Lee J.S., "BER Expressions for Differentially Detected π/4-DQPSK Modulation", *IEEE Transactions on Communications*, vol. 46, no. 1, January 1998.

[17] Dr. O.A. Sen, Sunay H.K., Ismailoglu A.N., Dudak C., Kırılmaz T., **"**High Data Rate X-Band Transmitter for LEO Satellites", *Symposium on Small Satellite Systems & Services (4S),* ESA-CNES, La Rochelle, 20-24 September 2004.

[18] Weisstein E.W., *Concise Encyclopedia of Mathematics*, *2nd Ed.*, Chapman & Hall/CRC, New York, 2002.

[19] Pinto J.L., Darwazeh I., "Effects of Magnitude and Phase Distortion in 8-PSK Systems on Error Vector Measurements", *Proceedings of 3rd Conference on Telecommunications (Conftele-2001)*, Figuera da Foz-Portugal, pp. 351-355, April 2001.

[20] Consultative Committee for Space Data Systems (CCSDS), Report Concerning Space Data System Standarts - Bandwidth Efficient Modulations, *CCSDS 413.0-G-1 Green Book,* April 2003.

[21] Rudge P.J., Gard K., Gutierrez H.M., Steer M.B., Miles R.E., "Modelling Spectral Regrowth and the Effect of Packet Size", *1999 High Frequency Postgraduate Student Colloquium*, 17 Sptember 1999, Leeds, England.

[22] Space Frequency Coordination Group Homepage, http:// www.sfcgonline.org, last accessed in August 2005

[23] Space Frequency Coordination Group, *SFCG Handbook*, Rec 21-1, 2002.

[24] Stoica P., Moses R., *Introduction to Spectral Analysis*, Prentice Hall Publications, 1997.

[25] Morais D.H., Feher K., "The Effects of Filtering and Limiting on the Performance of QPSK, Offset QPSK, and MSK Signals", *IEEE Trans. On Communications*, Vol. 28, pp. 1999-2009, December 1980.

[26] Cavers J.K., "The Effect of Data Modulation Format on Intermodulation Power in Nonlinear Amplifiers", *Vehicular Technology Conference, IEEE 44th*, Stockholm, Sweden, June 1994.

[27] Agilent Application Note, "Characterizing Digitally Modulated Signals with CCDF Curves", 2002.

[28] Cripps S.C., *RF Power Amplifiers for Wireless Communications*, Artech House Publications, 1999.

APPENDIX A

ROOT-RAISED COSINE FILTERING

In literature, Nyquist pulse-shaping criterion is very well known for distortionless baseband data transmission, [2], [11]. A particular pulse spectrum that has desirable spectral properties and has been widely used in practice is the raised cosine spectrum given as [2]

$$P(f)=\begin{cases} T & \left(0 \le |f| \le \dfrac{1-\alpha}{2T}\right) \\ \dfrac{T}{2}\left\{1+\cos\left[\dfrac{\pi T}{\alpha}\left(|f|-\dfrac{1-\alpha}{2T}\right)\right]\right\} & \left(\dfrac{1-\alpha}{2T} \le |f| \le \dfrac{1+\alpha}{2T}\right) \\ 0 & \left(|f| > \dfrac{1+\alpha}{2T}\right) \end{cases} \quad \text{(A.27)}$$

where α is called the rolloff factor and takes values in the range $0 \le \alpha \le 1$. It mainly imposes the excess bandwidth occupied by the signal beyond the Nyquist frequency.

The corresponding time domain pulse, *p(t)*, having the raised cosine spectrum is

$$p(t) = \text{sinc}\left(\frac{\pi \text{t}}{\text{T}}\right)\frac{\cos\left(\dfrac{\pi\alpha t}{T}\right)}{1-\dfrac{4\alpha^2 t^2}{T^2}} \quad \text{(A.28)}$$

Due to the smooth characteristics of the raised cosine spectrum, it is possible to design practical filters for the transmitter and the receiver that approximate the

overall desired frequency response. If the channel is ideal (having unity frequency response over the pulse bandwidth),

$$P(f) = F_T(f)F_R(f) \tag{A.29}$$

where $F_T(f)$ and $F_{R(f)}$ are the frequency responses of the transmitter and the receiver filters. If the receiver filter is also matched to the transmitter filter,

$$P(f) = F_T(f)F_R(f) = |F_T(f)|^2 \tag{A.30}$$

and

$$F_T(f) = F_R^*(f) = \sqrt{P(f)} \overset{\Delta}{=} F(f) \tag{A.31}$$

The overall raised cosine spectral characteristic is split evenly between the transmitting filter and the receiving filter, [2], without taking into account the physical realizability of the filters for the time being. This filter is named as root raised cosine (RRC) filter and time domain response is

$$f(t) = \frac{4\alpha}{\pi\sqrt{T}} \frac{\cos\left(\frac{(1+\alpha)\pi t}{T}\right) + \frac{T}{4\alpha t}\sin\left(\frac{(1-\alpha)\pi t}{T}\right)}{1-\left(\frac{4\alpha t}{T}\right)^2} \tag{A.32}$$

APPENDIX B

BIT ERROR PROBABILITY CALCULATIONS

5.5 BPSK Bit Error Probability Calculation

Zero mean additive white gaussian noise (AWGN) probability density function used in our analysis is given as, [11]

$$p(x) = \frac{1}{\sqrt{2\pi}\sigma} \exp\left(\frac{-x^2}{2\sigma^2}\right) \tag{B. 9}$$

where σ^2 is variance of the gaussian distributed noise.

Obtaining decision points at the receiver end (sampling instants), bit error probability of BPSK modulation is found as

$$P_b = 1 - \int_0^{\infty} \frac{1}{\sqrt{2\pi}\sigma_x} \exp\left(\frac{-(x-\mu_x)^2}{2\sigma_x{}^2}\right) dx \tag{B. 10}$$

where μ_x is the mean of the sample points and σ_x is the standard deviation of the sample points' distribution.

In this expression, with a variable transformation as

$$\frac{x-\mu_x}{\sqrt{2}\sigma_x} = t \tag{B. 11}$$

the following equation is obtained:

$$P_b = 1 - \frac{1}{\sqrt{\pi}} \int_{\frac{-\mu_x}{\sqrt{2}\sigma_x}}^{\infty} e^{-t^2} dt \tag{B. 12}$$

This result can be expressed as

$$P_b = BER = 1 - \frac{1}{2}\operatorname{erfc}\left(\frac{-\mu_x}{\sqrt{2}\sigma_x}\right) \tag{B. 13}$$

where

$$\operatorname{erfc}(x) = \frac{2}{\sqrt{\pi}} \int_{x}^{\infty} e^{-t^2} dt \tag{B. 14}$$

5.6 QPSK/OQPSK Bit Error Probability Calculation

Using the same noise probability density function in the BPSK case, one can write the bit error probability of QPSK modulation as

$$P_b = 1 - \int_0^{\infty} \frac{1}{\sqrt{2\pi}\sigma_x} \exp\left(\frac{-(x-\mu_x)^2}{2\sigma_x^2}\right) dx \int_0^{\infty} \frac{1}{\sqrt{2\pi}\sigma_y} \exp\left(\frac{-(y-\mu_y)^2}{2\sigma_y^2}\right) dy \tag{B. 15}$$

where μ_x, μ_y denote the axial mean values of the complex baseband sample points and σ_x, σ_y denote the axial standard deviations of the same sample points.

In this expression, by using variable transformations with variables t_1, t_2 as in the BPSK case, the following equation is obtained:

$$P_b = 1 - \frac{1}{\pi} \int_{\frac{-\mu_x}{\sqrt{2}\sigma_x}}^{\infty} \exp(t_1) dt_1 \int_{-\frac{\mu_y}{\sqrt{2}\sigma_y}}^{\infty} \exp(t_2) dt_2 \tag{B. 16}$$

This result can, again, be expressed in terms of a known mathematical function if we utilize Gray coding for the data bits. Then, bit error probability is obtained as follows:

$$P_b = BER \cong \frac{1}{2}\left(1 - \frac{1}{4}\operatorname{erfc}\left(\frac{-\mu_x}{\sqrt{2}\sigma_x}\right)\operatorname{erfc}\left(\frac{-\mu_y}{\sqrt{2}\sigma_y}\right)\right) \qquad \text{(B. 17)}$$

Bit error probability calculation for OQPSK is the same as that of QPSK.

For very low values of P_b, it is difficult to obtain the BER by simulation. However, if we can get a good estimate of the mean and standard deviations, the analytical expressions (B.5) and (B.9) can be used to compute the BER.

APPENDIX C

WELCH SPECTRAL ESTIMATION METHOD [23]

Welch method is a spectral estimation method in which time domain signal data are segmented allowing an overlap and each is windowed prior to computing the periodogram. For a mathematical form, let

$$y_j(t) = y((j-1)K + t), \begin{matrix} t = 1,...,M \\ j = 1,...,S \end{matrix} \qquad \text{(C. 1)}$$

denote the j^{th} data segment. In (C.1), $(j-1)K$ is the starting point for the j^{th} sequence of observations. The value, in general, used for K in the Welch method is $K = M/2$ and 50% overlap between successive segments are obtained.

The windowed periodogram corresponding to $y_j(t)$ is computed as

$$\hat{\phi}_j(\omega) = \frac{1}{MP}\left|\sum_{t=1}^{M} v(t) y_j(t) e^{-i\omega t}\right|^2 \qquad \text{(C. 2)}$$

where P denotes the "power" of the temporal window $\{v(t)\}$,

$$P = \frac{1}{M}\sum_{t=1}^{M}\left|v(t)\right|^2$$

The Welch estimate of PSD is determined by averaging the windowed periodograms in (C.2).

$$\hat{\phi}_w(\omega)=\frac{1}{S}\sum_{j=1}^{S}\hat{\phi}_j(\omega) \qquad \text{(C. 3)}$$

The Welch estimator can be efficiently computed via the FFT, and is one of the most frequently used PSD estimation methods.

C.1 Utilized Spectral Estimation Methodology

In the simulations, 50% overlap between successive segments are used. The length of each segment is chosen to be 512 symbol for each modulation scheme. The total data length is composed of 2000 data segments.